PRELIMINARY MECHANICAL CHARACTERIZATION OF THE LOW-COST METAL 3D PRINTING

A Thesis

Presented to

the Faculty of the College of Graduate Studies

Tennessee Technological University

by

Hao Lu

In Partial Fulfillment

of the Requirements of the Degree

Master of Science

Mechanical Engineering

August 2020

AN ABSTRACT OF A THESIS

PRELIMINARY MECHANICAL CHARACTERIZATION OF THE LOW-COST METAL 3D PRINTING

Hao Lu

Master of Science in Mechanical Engineering

Additive manufacturing (AM), commonly known as 3D printing, is an advanced manufacturing technology that has developed rapidly in the past 30 years. Its advantage lies in the rapid prototyping and small-batch production. Today, metal AM is gaining popularity due to its high strength and industrial applicability. However, this technology has a high-cost barrier, and it is not affordable for several end-users due to its initial cost, maintenance/safety requirements, and trained operator needs. Lately, a few companies have developed a new type of filament that will work with any low-cost material extrusion printers. These new filaments contain metal powders mixed with polymers and could be used for producing metallic parts as the end product. This study presents the unique low-cost Metal Material Extrusion (MME) technology and its mechanical characterization. In this printing technology, a specimen is made by printing a Polylactic Acid (PLA) compliant metal powder composite filament and then sintered using an open-air furnace. During the sintering process, the bonding agent is removed and the metal powders are fused. In the end, the sintered product is a solid metallic part. In this research, the bone-shaped specimens were manufactured and the tensile stress of the pre and post sintered parts was tested. After getting the strain-stress data, the results were compared with a pure metal specimen fabricated by other methods. Overall, this research reports the preliminary mechanical characterization of MME technology.

TABLE OF CONTENTS

CERTIFICATE OF APPROVAL OF THESIS

PRELIMINARY MECHANICAL CHARACTERIZATION OF THE LOW-COST METAL 3D PRINTING

by

Hao Lu

Graduate Advisory Committee:

Ismail Fidan, Chairperson	Date
Andy Pardue	Date
Pingen Chen	Date
Michael Allen	Date
Khalid Tantawi	Date

Approved for the Faculty:

Mark Stephens, Dean College of Graduate Studies	Date

DEDICATION

This thesis is dedicated to the people who have supported me throughout my education.

Thanks for making me see this adventure through to end.

ACKNOWLEDGMENTS

I would like to show my appreciation to Dr. Ismail Fidan who is my graduate advisor and helped guide me during my Master's research at Tennessee Technological University. I would also like to thank Dr. Andy Pardue, Dr. Michael Allen, Dr. Khalid Tantawi, and Dr. Pingen Chen for their advice and support at various points during the research study. I would like to thank Dr. Mahdi Mohammadizadeh, Ankit Gupta, Seymur Hasanov since they have spent their free time to help me with writing this thesis.

This study has been made available and funded through the National Science Foundation Award 1801120, Smart Manufacturing for America's Revolutionizing Technological Transformation. This support is greatly appreciated.

The research studies reported in this thesis have been performed at 1) Additive Manufacturing Research and Innovation Laboratory, 2) Mechanical Engineering Senior Design Laboratory, 3) Material Science Laboratory, and 4) Cryogenics Laboratory. The support provided by the graduate students, faculty, and staff of Tennessee Tech is greatly appreciated.

LIST OF FIGURES

LIST OF TABLES

LIST OF SYMBOLS

Acronym	Meaning
AM	Additive manufacturing
ANOVA	Analysis of variance
ASTM	American society for testing and materials
CAD	Computer-aided design
CNC	Computer numerical control
CPS	Cyber-physical systems
CTE	Coefficient of thermal expansion
DED	Direct energy deposition
Df	Degree of freedom
DMD	Direct metal deposition
DMLS	Direct metal laser sintering
DOE	Design of experiments
E	Young's modulus
FDM	Fused deposition modeling
LOM	Laminated object manufacturing
MSE	Mean squared error
MPLA	Metal polylactic acid
NA	Not available
PA	Polyamide nylon
PDF	Powder diffraction file
PLA	Polylactic acid
PM	Powder metallurgy
R3D	Raise 3D
SLA	Stereolithography
SLM	Selective laser melting
SLS	Selective laser sintering
SSE	Sum squared error
STL	Standard triangle language
TD	Thermal degradation
TGA	Thermal gravimetric analysis
TIG	Tungsten inert gas
TMA	Thermo-mechanical analysis
UMS5	Ultimaker s5
UTS	Ultimate tensile strength
XRD	X-ray powder diffraction

CHAPTER 1: INTRODUCTION

1.1. Additive Manufacturing

Additive manufacturing (AM), also known as three-dimensional printing is defined by the American Society of Testing and Materials (ASTM) as a manufacturing process of making objects from digital 3D models. In this process, materials are added layer upon layer, as opposed to subtractive manufacturing methodologies [1]. AM is a combination of computer-aided design (CAD), modeling, and fabrication technologies to convert the materials into a solid piece layer by layer.

AM technology is an advanced manufacturing technology developed at the end of the 1980s [2]. It is a common technology for new product development for many manufacturing enterprises. It promotes product innovation, shortens the development cycles of the new product, and improves the functionality and overall properties of the products. Since the advent of this technology, it has been widely used in several industries. As an example, dentists use the printers to scan the outline of the patient's teeth and then copy out the appropriate correction mold.

AM technology is also known as Rapid Prototyping. It is an important part of Smart Manufacturing system that can accurately and quickly transform the designer's idea into a functional prototype or final product.

Generally speaking, the AM process includes five steps:

1. **Model generation:** Using CAD software or scanning equipment to generate a 3D model of the product.
2. **Data format conversion:** Converting the 3D model into an STL format file. STL, an abbreviation of "Standard triangle language", is a standard file type used in the AM field. It is a triangular grid to discretely approximate the surface of a three-dimensional solid model.
3. **Slicing:** Slicing of the 3D model into thin layers using a computer software tool by processing the layers into the G-code. This process is carried out in specific slicing software like Cura or IdeaMaker.
4. **Printing:** Sending the generated code to a 3D printer. The 3D printer produces the part according to the G-code layer by layer.
5. **Post-processing:** Some parts may require extra processes such as polishing, cutting, and sintering to remove extra layers or support materials.

As Table 1 shows, there are many types of AM technologies including (1) binder jetting, (2) directed energy deposition, (3) material extrusion, (4) material jetting, (5) powder bed fusion, (6) sheet lamination, and (7) vat photopolymerization [3][4].

Table 1**:** Classification of AM processes by ASTM International

Classification	Technologies	Materials	Energy
Binder Jetting	Indirect Inkjet Printing	Polymer/ Ceramic/Metal Powder	Thermal Energy
Direct Energy Deposition	Laser Engineered Net Shaping, Electronic Beam Welding	Metal Powder	Laser Beam, Electron Beam
Material Extrusion	Fused Deposition Modeling, Contour Crafting	Thermoplastic, Pastes	Thermal Energy
Material Jetting	Polyjet/Inkjet Printing	Photopolymer, Wax	Thermal Energy, Photocuring

Table 1(Continued)

Classification	Technologies	Materials	Energy
Powder Bed Fusion	Select Laser Sintering, Direct Metal Laser Sintering, Select Laser Melting, Electron Beam Melting	Polymer/ Metal/ Ceramic Powder	Laser Beam, Electron Beam
Sheet Lamination	Laminated Object Manufacturing	Polymer/ Metal Film	Laser Beam, Ultrasonic Vibration
Vat Photopolymerization	Stereolithography	Photopolymer, Ceramic	Ultraviolet Laser

- Binder jetting process deposits a liquid bonding agent onto a powder bed. The bonding agent infiltrates the surface of the powder bed and forms a solid structure. Then the roller is used to spray another layer of the powder on the top. The final product is made by repeatedly spraying the bonding agent and then the powder [5].
- Directed energy deposition (DED) is an AM process that directly feeds the material into the focal point of the energy beam. Raw material can be a powder or a filament, which is sent into the path of a laser or electron beam and melts as the material is deposited [6]. The DED process is like using a TIG welding machine to do the printing.
- Material extrusion process is one of the most commonly used AM processes. It is low cost and highly popular in several applications. The Fused Deposition Modeling (FDM) fabricates the parts by mechanically extruding the molten thermoplastic material from an extrusion head. Another type of material extrusion process is paste extrusion (e.g., TechBot [7]). It typically uses slurries (e.g., frosting, clay, or cement) for extrusion through a syringe-like deposition head [4].
- Material jetting deposits a layer of resin onto the printing bed, then solidifies the resin via heat or UV light rather than using a bucket for selective curing [8]. The

way material jetting sprays the resin is similar to a regular 2D printer's inkjet. The difference is the resin will solidify and makes it serve as the foundation of the next layer so that the layers will be superimposed to form a solid, while the ink can only penetrate the material and stay on the same plane.

- Powder bed fusion is an AM technique designed to use a high-power laser or electron beam to fuse the powder. After the laser fuses the powder in the current layer, a rolling mechanism spreads the powder for the next layer [9]. SLS, DMLS, and EBM are the most popular metal powder bed fusion techniques. This technique can be used for processing metal, polymer, and ceramic materials [10].
- Sheet lamination is known as laminated object manufacturing (LOM). LOM is an AM technology which is also based on subtractive manufacturing. LOM cuts a thin film of material into the desired shape for the layer and adheres the layers with the help of bonding agent. It can use plastic, metal, or even paper as raw materials [11]. The printing speed of this technology is fast but it will produce a lot of waste compared to other AM technologies [12].
- Vat photopolymerization is the stereolithography method (SLA) utilizes photosensitive resin as raw material. The photosensitive resin is generally in the liquid state and it immediately causes polymerization reaction under the irradiation of a certain wavelength of UV light to cure. SLA uses a specific intensity laser to focus on the surface of the resin so that it can produce a solid piece by curing the resin layer by layer. This technique can also be used for producing porous bio-ceramics with high resolution and low surface roughness [13]. One group of

researchers processes ceramic components form alumina by suspending particles in the resin to create a ceramic part with 43.3% porosity [14].

1.2. History of AM

AM's history started in the late twentieth century [15], but some of the ideas behind it can be traced back to the eighteen century. In 1859, French photo sculptor Francois Willeme created one of the earliest 3D images by using multiple cameras to take a picture of subjects from different angles [16]. 33 years later an inventor created a 3D topographic map by using the layering method [17]. In 1980, Dr. Hideo Kodama invented a photopolymer rapid prototyping system by using UV light to cure the photosensitive polymer [18]. A few years later, in 1986, Chuck Hull patented stereolithography which uses UV to cure a photosensitive polymer layer by layer to create a 3D object [19]. Later, he started a company and launched the SLA-250, the first large volume commercial 3D printer. He also created the STL file format which is commonly used in the AM field today. From here, AM technology developed rapidly. A year after the first commercial AM system launched, S. Scott Crump filed a patent for FDM [20].

As the AM technologies develop the 3D printer's size became smaller, the unit price got cheaper, and the printed product's geometry also got more complex as the designer kept pushing the envelope of design. AM technology has developed rapidly in recent years, and is currently used in automotive manufacturing, medicine, machinery, biology, aerospace, electronics, and other fields, and has achieved significant results. In 2005, the first self-replicating printer launched [21]. In 2012, the first 3D chocolate printer

'Choc Edge' was launched [22]. In 2013, a US company, Organovo created the world's first fully cellular 3D bio-printed liver tissue [23]. In the same year, the open-source firm, Defense Distributed organization, designed a gun and released the plans on the Internet. In 2014, Strati, the first electric car to utilize AM during the production process, was manufactured by Local Motors and Cincinnati Inc during the 2014 International Manufacturing Technology Show in Chicago, Illinois [24].

After several decades of development, AM has become the technology that everybody can see in every aspect of daily life. Figure 1 represents the schematic of historical developments of AM technology from the 1950s to today.

1.3. Background of Metal AM

One of the earliest AM technologies related to metal additive manufacturing is SLS. SLS process was invented by Carl Deckard in 1989. It uses laser as the power source to sinter powdered material (typically polymers) to create a solid structure. In 1990,

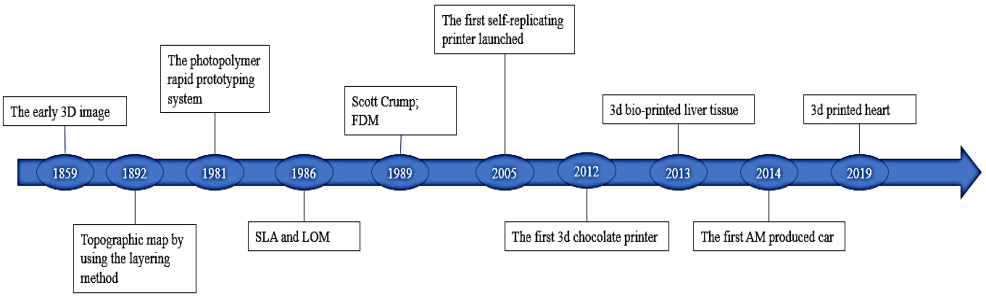

Figure 1: Timeline of additive manufacturing technology [25]

Manriquez-Frayre and Bourell realized the application of printing metal products through SLS technology [15]. To this day, when we talk about metal AM, we usually refer to SLM, DED, and EBM.

Both SLM and EBM are powder bed fuse AM technique. DED is a metal AM technology which is similar to the SLM. DED melts the wire/powder by electron beam, plasma or laser, and fusses material as it is deposited to produce the product [6]. Those metal AM methods have a common feature: expensive equipment and complicated operation training. This is not the cost that a person or organization can easily afford.

1.4. Advantages of AM

There are many advantages of using AM. AM technologies can directly use product design data to quickly fabricate the prototypes. Further advantages are highlighted below. Overall, AM can

- provide more flexible product design and rapid prototyping, which can reduce the cost of developing and producing complex-shaped products
- eliminate the sub-assembly requirements of complicated products by producing a fully-assembled product
- reduce the waste of material in the production process to reduce cost.

Today, it is projected the AM market will grow to $21 Billion [26]. The technology also stimulates the development of the maker movement by democratizing design and manufacturing [27]. Smart manufacturing is also a hot topic which has attracted interest of

many industries. With this trend, AM technology is precisely in line with this tendency. Compared with conventional manufacturing, AM has advantages summarized as follows [28]:

- After years of development, the accuracy and surface finish of the final products from AM have been greatly improved.
- The production cycle is short. Traditional model making often needs to go through the process of mold design, production, and trimming, and the production cycle is long. AM eliminates the manufacturing process of the mold and greatly shortens the production time of the model. Generally, a model can be printed in a few hours or even tens of minutes.
- The labor requirements in AM are very minimal compared to the conventional manufacturing processes. However, sometimes AM parts need post-processing.
- A wide range of raw materials can be used for AM processing, depending on the application. Most AM materials are polymers, photosensitive resins, metals, composites and ceramic materials. In recent years, cement, biomaterials, *etc*. are also been used in AM processing [29]–[33].
- The technology could produce very complex parts from several different materials in a short period and make it ready for functional uses. Such a unique solution will help the manufacturers produce versatile products with low-cost limits [22].
- There is a reduction in the overall cost of the supplies and consumables of AM today. Such a growing trend in AM is helping the market to be competitive in producing low-cost products [34].

1.5. Advantages of Metal AM

In recent year metal AM technology has found its way in various engineering fields such as aerospace, automotive, and defense. It has been used in the fabrication of a wide range of commercial functional applications. In particular, nowadays metal AM is popular in the aerospace industry to build and repair various components. Like other technologies, metal AM has advantages and disadvantages. The advantage of metal printing is that it can create high-strength, light-weight, and complex parts [35]. It can also produce internal complex structures that cannot be processed by any traditional manufacturing processes. Moreover, it produces minimal material waste [36]. Determining the optimized printing parameters is important to attain a high-performance part. Once the parameters are determined, the part can be made repeatedly.

The aerospace and automotive industries are the early adopters of this technology, and the high-strength while light-weight AM product meets the needs of these industries [28]. At present, the commonly used metal materials include stainless steel, aluminum alloy, titanium alloy, cobalt-chromium alloy, *etc*. [37]. The selection of the suitable material is critical to the ability of the part to meet the requirements of the specific application.

Metal AM technology also has some disadvantages. Due to the layer-by-layer manufacturing, some areas of the product may need to have support while being printed. Also, metal printed parts often have poor surface quality and require CNC's secondary processing or manual sanding and polishing [38]. Moreover, these processes can only be limited to the areas that can be reached by the processing tools. Compared to conventional AM like FDM and SLS, metal printing takes longer, and it usually requires a further step

like heat treatment. Although metal AM is not as easy as plastic printing, due to the high process requirements and obvious advantages, it is worthwhile to further investigate the design, process, and post-processing relationships [39].

The aerospace industry has invested in AM to develop customized parts with higher strength-to-weight ratios, as well as for quick maintenance of aircraft and on-demand manufacturing [40]. However, the adoption of AM in the aerospace industry faces challenges such as limited materials and high cost [41]. The main disadvantages are the high cost and reduced mechanical properties compared to traditional methods that have severely limited the promotion and applications of metal AM [42]. Although there are several benefits of adopting metal AM, there are still some disadvantages that require further investigations like the high cost of materials, the porosity of finished products, and the initial cost of the machine. Despite being a revolutionary method for customized products and applications, AM needs more development to compete with the traditional methods in the mass production of products. Nonetheless, the evolution of AM in recent years has been phenomenal. The increased funding, research, and development worldwide will result in a fast transition from traditional methods of manufacturing to metal AM soon.

1.6. Significance of the Research Study

At the fourth industrial revolution, AM is one of the branches of Smart Manufacturing. The concept of AM gradually improved the process of traditional manufacturing. AM cannot currently replace the traditional manufacturing processes since each process has its niches, *ie*. CNC for accuracy and casting for large-sized production.

Traditional manufacturing depends on large-scale production equipment, workers, and assembly lines. For the future, Smart Manufacturing is the goal for 21st-century manufacturing [43]. Smart Manufacturing uses Cyber-Physical System (CPS) to digitized supply, manufacturing, and sales information to achieve a fast, effective, and personalized product supply chain. Continuous development of new technologies and new materials is expected to allow AM to enter into various industrial fields.

Nowadays, AM has received more and more attention. However, most metal printing requires expensive equipment and many cumbersome operations. The metal printing method used in this study is a production method that simplifies the operation and reduces the cost of the entire production. This technology requires only a common FDM desktop printer and a filament warmer.

This research demonstrates the practicality of this printing technology and compares it with other production technologies. AM technology and its industry are still far from the mature stage. It is believed that innovative research and long-term technology accumulation and verification are still needed to create a low cost and readily available AM machine for printing [44].

Several common methods of metal printing; *i.e.* DMLS, SLM, and DMD all require expensive equipment [45]. For individuals or small companies to make parts with several customer requirements, these methods are too expensive. The alternative method as mentioned above is the material extrusion technology to produce relatively cheap metal parts, which has become a rigorous study in this field [46]. The method involves fusing a polymer and a metal powder composite to produce a filament. This filament can be widely used in any commercial-grade 3D printers like ordinary PLA. The final part can then be

sintered to produce full metal parts. MME is an emerging field and must be understood to better characterize the material properties of this manufacturing technology.

1.7. Selection of Metal AM

Producing metal AM parts, as the most cutting-edge and promising technology in advanced manufacturing, is an important direction of 21st-century manufacturing. It has been listed as one of the top ten breakthrough technologies of 2018 by the MIT Technology Review [47]. At present, several methods that can be used to directly manufacture the functional metal parts could include SLS, DMLS, and DED.

Material extrusion creates the product by pushing a filament through a heated nozzle shown in Figure 2. The filament reaches the liquid state as it passes through the heated nozzle and is extruded onto a heated bed [4]. By taking advantage of the properties of thermoplastics this allows the filament to be fused during printing and then solidify at room temperature after printing. Low cost, high speed, and a simple process are the main advantages of the material extrusion process. On the other hand, low mechanical properties, poor surface quality, and a limited number of thermoplastic materials are the disadvantages of the material extrusion process. The parts produced by material extrusion may require post-processing to be functional. The material extrusion process has lower accuracy compared with other AM methods [48]. Overall, it takes extra time to make the final products after sintering and surface finishing.

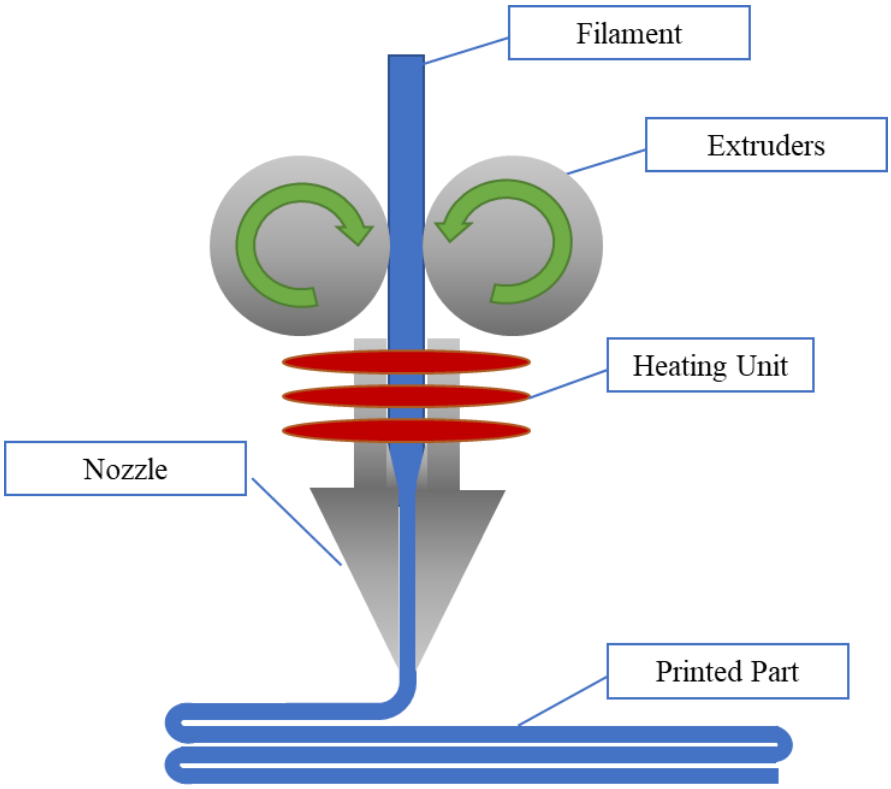

Figure 2: Schematic view of material extrusion process

There are three main methods of material extrusion printing and they are as follows: Cartesian (CoreX/Y/H-bot), Delta, and Polar.

Cartesian *(CoreX/Y/H-bot)*: This is the most common design in consumer-level 3D printers. It typically has a print bed that moves only in the z-axis. And the extruder moves in the X/Y axis. The Cartesian 3D printers have heavy moving parts. It is difficult for Cartesian printers to stop or change orientation immediately [49]. Constant shaking of the platform can cause loose and inaccurate printing, especially when the print volume becomes high. However, it has an excellent printing effect at the horizontal level, easy to learn kinematics, and consumer-friendly. The cubic frame is easy to encapsulate in most models, the mechanical structure is simpler, and the system is easier to maintain.

Delta: The delta structure has the same structure as the parallel robot. It uses three arms with parallelograms to maintains the orientation of nozzle. Because of its fast speed, strong flexibility, and other advantages, this type of structure becomes popular in 3D printing. The delta structure can print a product with greater height [50]. Delta's disadvantage is the slight lack of printing accuracy [51].

Polar: This structure is similar to the cartesian structure except the extruder uses the polar coordinate system instead of the cartesian system. The bed spins and moves in the z-axis. It has a larger build volume and is the simplest design compared to the Delta and Cartesian structures [52].

1.8. Sintering Process

The parts fabricated by the AM techniques such as Binder Jetting and MME are called a “green part”. The mechanical properties of these green parts are extremely poor [53]. Sintering these green parts increases the density but reduces the geometric accuracy. The part is then machined to obtain the desired geometry. In a way, the sintering process refers to the transformation of powdered materials into a dense object. The manufacturing industry has used this process to produce ceramics, refractory materials, metals, and so on for several years [54]. Figure 3 shows the process of sintering: The powder material is formed into a certain shape (A). Then during the temperature rise the powder particles start to expand and fuse (B). Finally, shrinkage of the part during cooling and making a part with little void (C) [55]. The sintering process directly affects the grain size, pore size, and grain boundary shape and distribution in the microstructure, which then affects the

performance of the material. The larger the particle size, the more the porosity [56]. Sintering often requires high temperatures for the reaction to proceed efficiently, but it performs at temperatures below the melting point of the material to ensure a uniform phase. The mechanical properties decrease if the sintering temperature decreases [57]. In many cases, sintering needs to be performed in a specific gas or vacuum environment and at an elevated temperature.

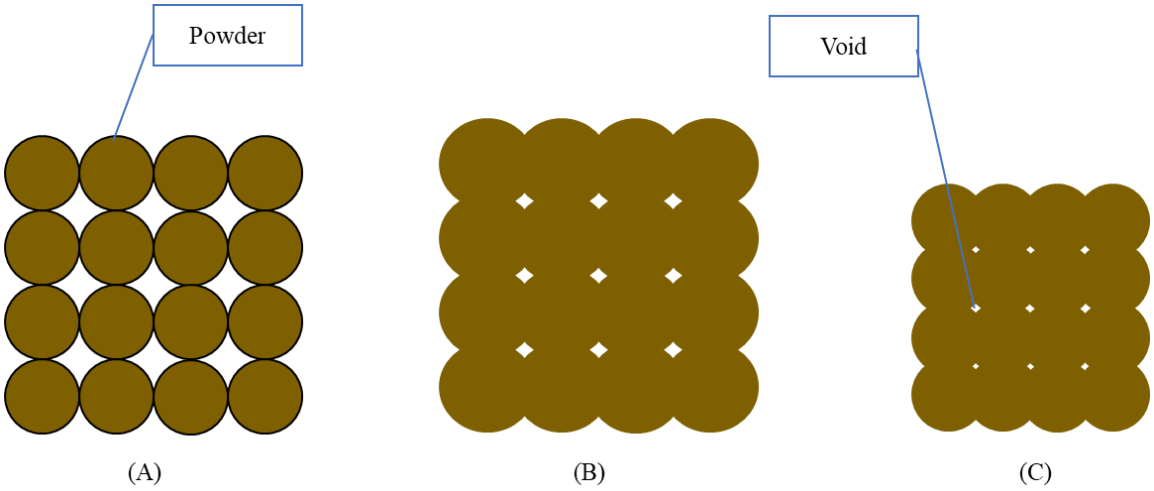

Figure 3: Sintering process (A) form shaping (B) expansion and fusion (C) Cooling

CHAPTER 2: LITERATURE REVIEW

Today, it is possible to produce complex metallic workpieces with MME techniques. Compared with the traditional molding methods, advancing AM processes makes the manufacturing a shorter amount of time and at a lower cost [58]. Eventually, MME techniques will contribute to the metal manufacturing processes by making more complex parts in a shorter amount of time and at a lower cost. However, AM will not completely replace traditional manufacturing [44].

Generally, the layer thickness and orientation of printing affect the mechanical properties of the AM processed parts. Fernandez-Vicente et al.'s research shows that the influence of the different printing patterns causes a variation of less than 5% in maximum tensile strength. The change in infill density mainly determines the tensile strength. The combination of a rectilinear pattern in a 100% infill shows the higher tensile strength [59]. Rankouhi et al. performed tensile testing on the ABS polymer material with different layer thickness and printing orientation. The results showed that higher layer thickness has lower ultimate tensile strength (UTS) because the air-gap size was proportional to the layer thickness [60]. Khalid Rafi et al.'s performed the experiments on Ti–6Al–4V and 15-5 PH steel using the SLM process. The samples' tensile properties were compared with respect to the printing orientation. The horizontally built samples showed relatively better tensile properties as compared with the vertically built samples [61]. Buchanan et al. studied the stress-strain behaviors of the Powder Bed Fusion AM martensitic stainless steel and 316L stainless steel structures. The research showed that the measured tensile strengths were found to be generally higher than conventionally formed material and the Young's modulus

(E) was generally lower than traditionally manufactured parts [62]. Material layer thickness and raster orientation have a significant effect on mechanical properties. Tensile test results showed that in the case of polymer, lower layer thickness exhibits higher elastic modulus and ultimate strength compared with higher layer thickness [26]. Similar results are shown in Kai et al.'s research on SLM produced 304 stainless steel parts' tensile properties. They also found that the overlap rate and slice thickness does not affect tensile properties [63].

Nowadays metal AM is focused on printing the metal or ceramic powders, failure behaviors of the part produced and life predictions of 3D printed parts, establishing standard specifications for non-destructive testing of 3D printed parts and mechanical characterization [26]. Spierings et al. found out that during the AM process the alloys are repeatedly heated and cooled. This repetition adds complexity to the microstructural characteristics. After the annealing treatment and machining operation, the parts may present the fatigue performance equivalent to that of machined metallic parts [35]. In some cases, the metal AM produced part may have higher mechanical properties compared to other manufacturing processes, such as aluminum alloy and stainless steel. Bian et al.'s research showed that the aluminum alloy printed by using direct metal laser sintering has better mechanical properties than casting piece due to the finer grain size [64]. Jordan et al. performed a series of property tests on SLS and SLM parts. Density tests and bending tests proved the ability of SLS/SLM to produce parts with good mechanical properties [58]. Wang et al. compared the mechanical properties of the two most common metal AM techniques: SLM and DMD. The result showed that both AM produced parts are stronger than traditionally manufactured parts but elongation at break value is much lower. They

showed that the SLM and DMD processes are suitable for complex internal structures and large-scale manufacturing, respectively.

Metal AM parts also have residual stress problems. Metcelis et al. found that the residual stresses in SLS and SLM parts are very large. The most important parameters determining the magnitude and shape of the residual stress profiles are the material properties, the laser scanning speed, and the heating conditions [65].

In recent years there are filaments made by metal powder and polymer. Very few scholars have conducted research on this topic. Hwang et al. used the ABS-Cu and ABS-Fe composite filaments in their studies. The tensile strength and strain of their products were reduced by decreasing the viscosity of ABS. Both the tensile strain and stress were decreased by raising the content of metal particles. Fill density also influences the tensile properties, it was observed that the tensile strengths decrease with the fill density [66]. Masood et al. found the thermal conductivity of metal/polymer composite filaments is sensitive to the amount of metal filler. As the volume percentage of the metal filler increases, the thermal conductivity increases significantly [67]. These special filaments will form a metal part by going through the sintering process. Riecker et al. produced their filament made by Polyamide-Nylon (PA) matrix with metal powder. The filament can be utilized by any low-cost desktop system to produce a part. After the thermal debonding and sintering process, the user can receive a metal part [68]. In the last few years, several companies (i.e. BASF and Virtual Foundry) have developed a new type of filament which could be used for digital fabrication of any given workpiece using any FDM-type desktop printer. After the debonding and sintering processes, the user of this technology is left with an additively manufactured part produced with nearly 100% solid metal [69]. The main

advantage of low-cost metal 3D printing with metal powdered filaments is to allow it for production of complex shapes and 3D printing with more than one metal at a time. In a normal foundry setting, it is not possible to cast two metals at the same time. The other advantage of low-cost metal 3D printing is that it is a safer solution than SLS process since there is no chemicals used in the FDM printing process [70].

Gong et al. reported a comparative study for producing Stainless Steel 316L parts via SLM and FDM technology using metal-polymer composite filament. In the research, several tests were performed to investigate the material properties and part shrinkage [71]. Pioneering studies performed on the dimensional variation, surface roughness, and microstructural analysis of sintered and un-sintered parts made through low-cost metal 3D printing technology were reported by Terry in 2019 [72][73]. Bin Liu et al. also studied the mechanical properties of FDM made metallic parts. Their study used the FDM process to create a green part that would then undergo debonding and sintering in a protective gas environment to form a fully finished metallic part. Due to the porous structure, though, it was observed that the tensile strength was not as high as SLM parts [74].

There are many parameters of the sintering process that have effects on mechanical properties such as porosity, particle size, sintering temperature, and holding time. Wang et al. found that as the sintering temperature and sintering holding time increase, the shear stress increases [75]. This shows that the tensile stress is proportional to temperature and holding time.

Metal Additive Manufacturing has attracted much attention in recent years. Many researchers are using their potentials in this field to move this technology toward industrial production. It has gathered tremendous attention from the aerospace, medical devices, and

defense sectors. However, the main drawback of metal additive manufacturing has been the high cost of production, which originates from the expensive machines and equipment used for this method. In this research, a low-cost manufacturing method for metal AM is introduced. The method is based on the FDM process with a price much lower than the laser-based Metal AM processes.

In the presented method, a mixture containing powdered metal and a polymer is printed using the FDM process. Then, the product is sintered at high a temperature. Sintering at high temperature leads to 1) degradation of the polymer phase, 2) improving the mechanical performance of the product. This research opens a door for low-cost AM of metals. The question answered by this research is "what are the mechanical and thermal properties of the part produced with low-cost metal AM?"

To answer this question, the specimens were prepared using PLA as the polymer and Cu, Al, Br, HC, and SS as the base metal in powder form. The mechanical properties of the specimens were studied using tensile and compression analysis and the thermal properties were examined using the Thermo-mechanical analysis (TMA), and thermo-gravimetric analysis (TGA) method. The microstructural analysis was used to study the morphology and void contents of the specimens.

CHAPTER 3: EXPERIMENTAL STUDIES

This section includes the thermal and mechanical analysis performed during this research study. The tensile and compression analysis was conducted to study the mechanical performance of the MME specimens. TGA and TMA were used for thermal analysis of the MME specimens. The optical microscopy and SEM tests were conducted to investigate the microstructure, morphology, and void in the structure.

3.1. Equipment and Materials used for Sample Preparation

In this section, the process, types of equipment, and materials used for the fabrication of MME specimens are discussed. The process of manufacturing the parts by low-cost MME is similar to the conventional FDM printing process. Figure 4 demonstrates the flowchart of the process. As can be seen, the process includes the following steps of CAD modeling, STL file generation, slicing, filament warming, material extrusion, sintering, and post-processing.

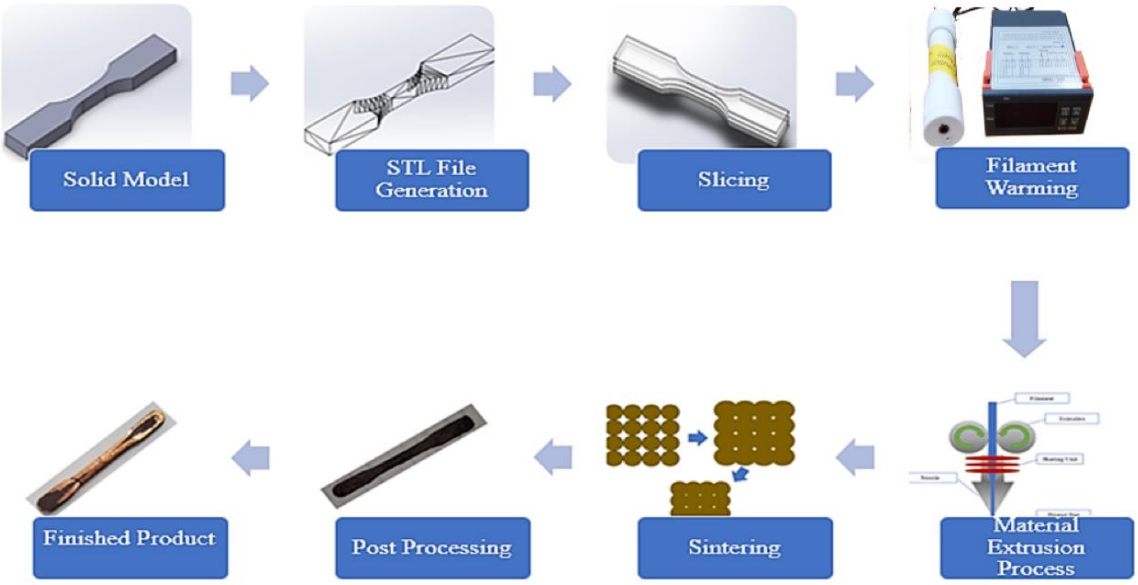

Figure 4: Low-cost metal material extrusion process

3.1.1. Filaments and Filament warmer

The filaments required for metal 3D printing were obtained from the Virtual Foundry [76]. Filament composition includes polylactic acid (PLA) polymer, metal powder, and a small amount of bonding agent as shown in Figure 5. The presence of PLA as the main carrier and bonding agent makes the fabrication of parts possible by FDM technology. The materials used in this study can be classified according to the type of metal powder contained. Filaments with metal particles studied in this research were Copper (Cu), Bronze (Br), Stainless Steel (SS), High Carbon Iron (HC), and Aluminum (Al). Filaments with Cu, Br, and SS metal particles were 2.85 mm in diameter and filament with HC and Al metal particles were 1.75 mm.

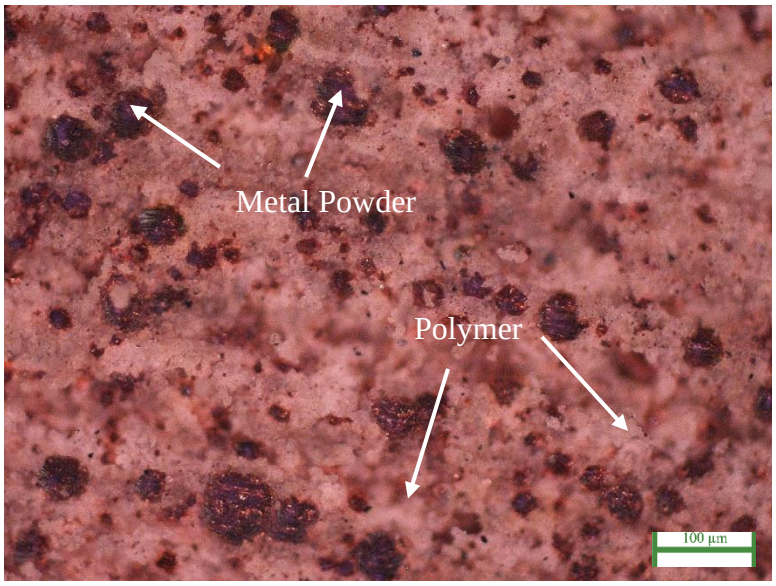

Figure 5: Optical microscopy image of un-sintered copper PLA

The filaments used in this research have high metal content which makes it more brittle and it is likely to break inside the Bowden-tube of 3D printer during the printing process. So, in order to avoid this excessive brittleness of metal filament, filament warmer was used to impart small amount of ductility to the filament. Figure 6 demonstrates the filament warmer used in the research. The filament warmer heated the filament to the temperature range of 55-60 C. This temperature is high enough to improve the ductility of the filament. So, the filament passes through the Bowden-tube of 3D printer without fracture. After printing, the part needs to be sintered and polished to get the smoother surface.

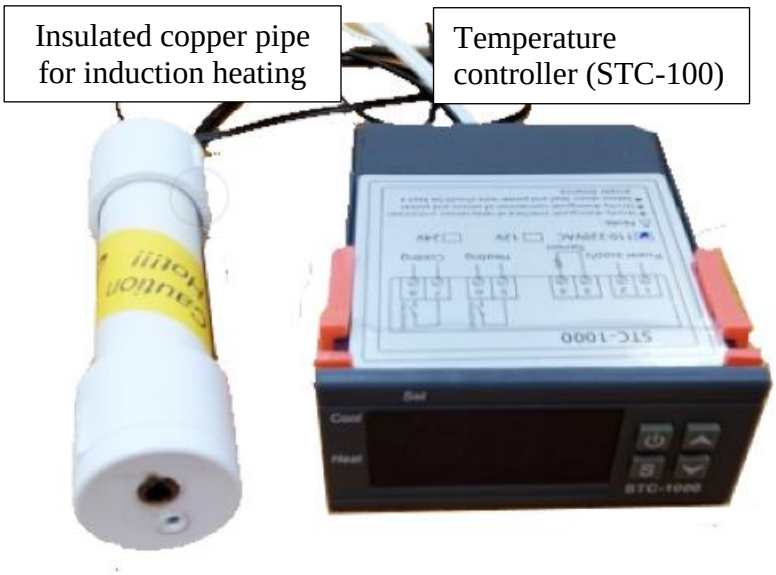

Figure 6: Filament warmer

3.1.2. 3D Printer

In this research study, Ultimaker s5 (UMS5) and Raise 3D pro2 (R3D) were used as 3D printing machines to make the metal-based printed specimens. Both printers are based on the Cartesian structure. UMS5 is a Bowden-drive printer that utilizes 2.85 mm diameter filament. R3D is a direct-drive printer that utilizes 1.75 mm diameter filament. The 0.6 mm ruby nozzle and hardened steel nozzle were used for machines, respectively. The layer resolution is greater than 100 micrometers. Both printers' minimum feature is 0.6 mm due to the nozzle size.

As the metal powder occupies a large proportion in the filament, the filament cannot be extruded with regular PLA-printing temperature. So, the printing temperature needs to be increased in order to reduce the viscosity of PLA and maintaining the required flow rate.

3.1.3. Furnace and Sintering Process Settings

Induction furnaces were used for the sintering of 3D printed metal parts. First, the furnaces' temperature is increased with two different temperature rates. Then, the specimens were sintered at a constant temperature of 1065 C in order to complete the sintering process. In this process, accurate control temperature is critical. Figure 7 demonstrates two furnaces (Lindberg Blue M, and KSL1100X) used in this research. The specifications of both the furnaces are shown in Table 2.

Figure 7: The Furnaces used in research: KSL1100X (a) and Lindberg Blue M (b)

Table 2: Specifications of the furnaces used in the research study [77][78]

Model	Capacity	Max (C)	Exterior (D×W×H)	Control	Electrical
Lindberg Blue M	16.4 L	1200	58.4 x 61 x 68.6 cm	Digital programmable control with 4 stored programs, 16 segments per program, and RS-232 communications interface	208/240 V, 50/60 Hz 4500 W, 16-19 A
KSL1100X	1 L	1100	23 x 20 x 36cm	30-segment, programmable temperature controlle	110V 950 W

Lindberg Blue M was used as the primary furnace with a maximum temperature of 1200 C, and with a larger volume compared with the KSL1100x. KSL1100X is a compact muffle furnace with a max temperature of 1100 C.

During the sintering process, Al_2O_3 powder was used as ballasts. The ballast is to support the shape of the part and keep the specimens to stay in the middle of the container for uniform heating. In the first step, the specimen was heated to 60 C in order to remove moisture and volatile contents. Then, the temperature is raised to 300 C at a rate of 2 C/min, which leads to the degradation of PLA polymer material and other bonding agents. After the degradation is finished, the temperature is increased at the same rate to 1015 C. Then, the temperature is increased again but at a lower rate of 25 C per hour to obtain a temperature of 1065 C. Then the samples are allowed to stay at this temperature for at least 7 hours for allowing the metal powder to expand and fuse with the neighboring particles. After the completion of the sintering process, the specimen is post-processed to remove the oxidation layers and the remaining ballast. The resultant part is pure metal parts with no polymer material, bonding agent, and other foreign particles.

Figure 8 demonstrates the variation in the furnace temperature during the entire sintering process. Furnace temperature segment settings are briefly explained in Table 3.

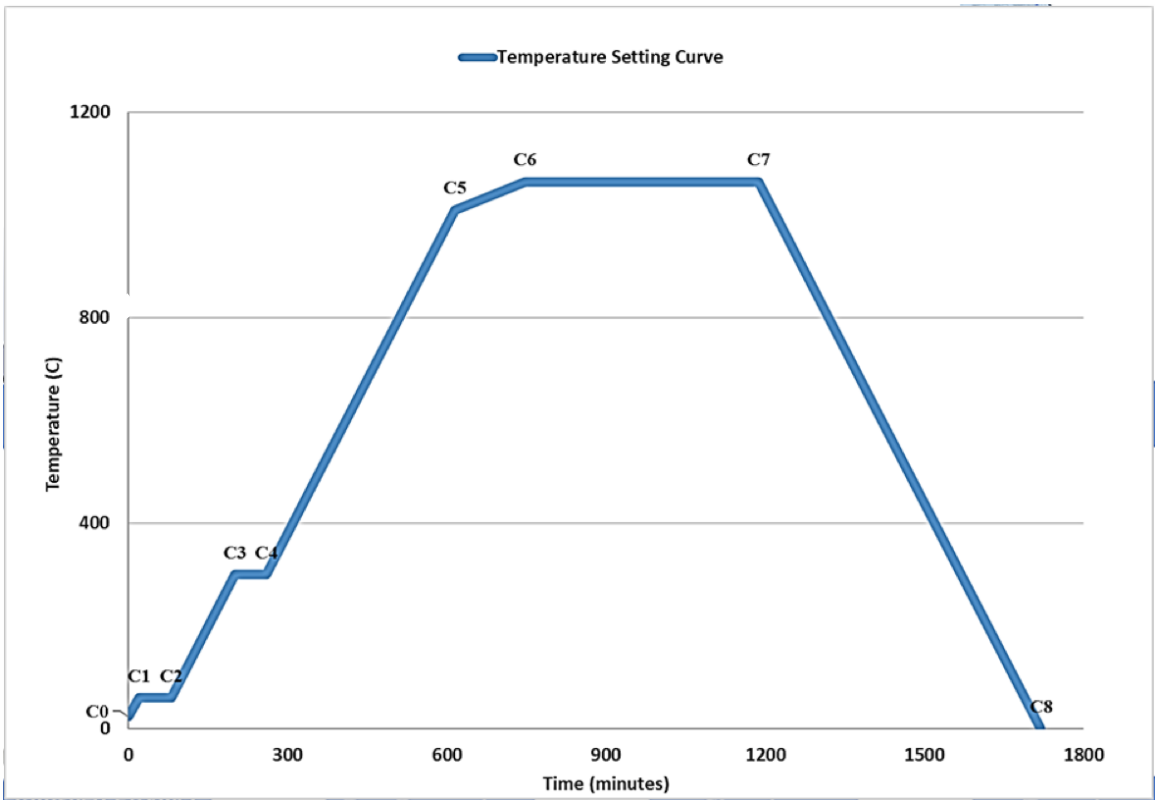

Figure 8: Furnace temperature process

Table 3: Temperature segment setting

Prompt	Input temperature values	Description
C0	23	Initial temperature
C1	60	Target temperature of the first heat-up stage
T1	20	Heat-up time 20 minutes from 23-60C in the first segment
C2	60	Target temperature of the second stage
T2	60	Keep 60 minutes at 60 C in the second segment
C3	300	Target temperature of the third stage
T3	120	Heat-up time 120 minutes from 60-300 C in the third segment
C4	300	Target temperature of the fourth stage
T4	60	Keep 60 minutes at 30 C in the fourth segment
C5	1010	Target temperature of the fifth stage
T5	355	Heat-up time 355 minutes from 300-1010C in the fifth segment
C6	1065	Target temperature of the sixth stage
T6	132	Heat-up time 120 minutes from 1010-1065 C in the sixth segment
C7	1065	Target temperature of the seventh stage
T7	440	Keep 440 minutes at 1065 C in the seventh segment
C8	0	Program end, Out-put power off. Furnace cooling down naturally.

3.2. Thermal Analysis

TMA and TGA were conducted to study the thermal properties of the MPLA filament. TMA was conducted to determine the coefficient of thermal expansion (CTE) and Thermogravimetric Analysis (TGA) was conducted to determine the metal ratio in the specimens and thermal degradation temperature.

3.2.1. Thermogravimetric Analysis (TGA)

TGA is one of the thermal analysis methods in which the mass of a sample is measured over time as the temperature increases with the defined rate. TGA curve can be used to study the thermal stability and composition of the material. In this research study, TGA is used to measure the thermal decomposition temperature of the polymer and the true weight percentage of the metal. Using this test, the thermal stability and rate of decomposition of specimens were measured. The test was conducted according to the standard ASTM E1131 [37].

Figure 9 shows a picture of TA Instruments SDT Q600 model used for this test. There are two pans in the machine: sample pan and reference pan. Both pans are installed on the balance arm with a thermocouple located in the furnace's chamber. 50 mg of the sample was loaded into the sample pan. Then the furnace was allowed to close in order to heat the sample from room temperature to 700 C at a constant rate of 10 C/min. As the Al-PLA filament contained aluminum alloy material with melting point of about 600 C, to

prevent damage to the sample pan, the final temperature was set to 500 C for the aluminum parts. Figure 10 shows the powder form of MPLA samples used for this test.

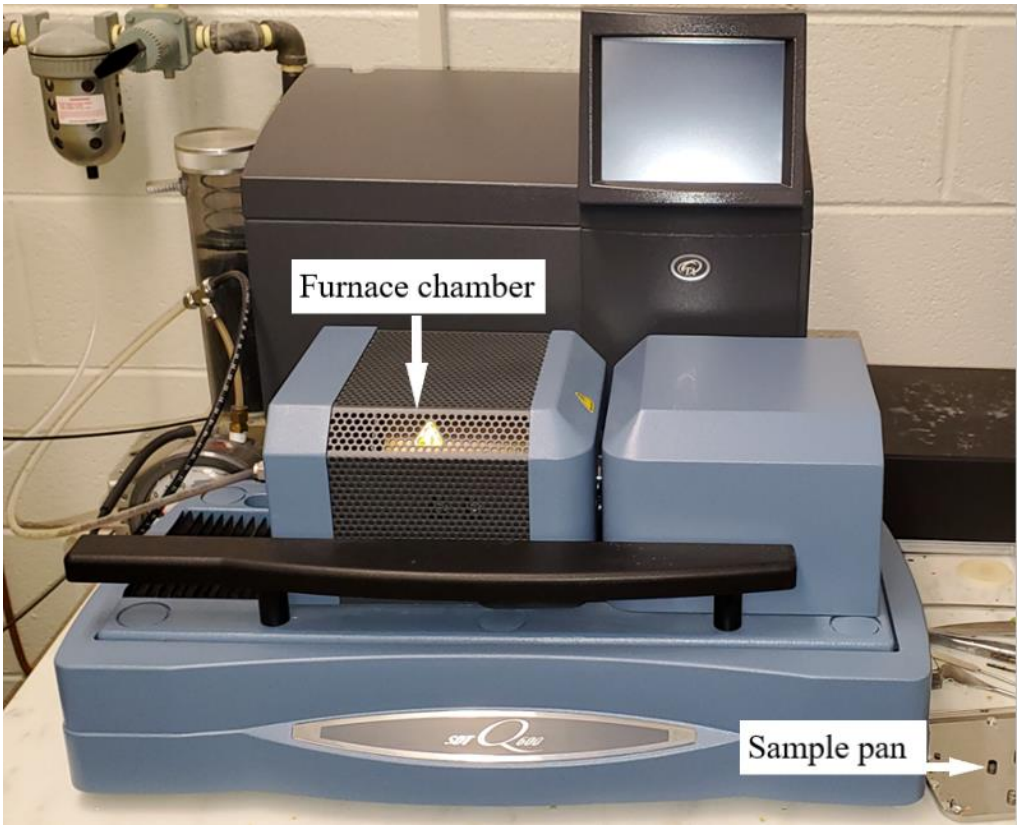

Figure 9: TGA tester: SDT Q600

Figure 10: TGA test samples (a)filament pieces (b) filament powder

3.2.1.1. TGA Results

During the testing process, the sample weight was recorded continuously as the temperature increased. Cu-PLA, Br-PLA, SS-PLA, Al-PLA, and HC-PLA filaments were used in this test. Each test was repeated two times. Figure 11 shows the TGA curves of all five MPLA filaments. The TGA gives detailed information about the degradation temperature and rate of decomposition. Figure 11 demonstrates that all five specimens degrade in the approximate range of 300-400 C. So, the furnace temperature for degradation of the polymer phase was set at this range for two hours. As can be seen, each curve exhibits the mass loss per degradation temperature thereby giving the degradation rate.

All MPLA filaments' decomposition temperature and residues are listed in Table 4. The decomposition temperatures are in an approximate range from 230 to 300 C. All the curves after approximately 430 C tend to be horizontal until the end of the test. The horizontal part of the curve at high temperature shows the residue content. The residue represents the metal content weight percentage. Table 4 shows that the thermal degradation temperature for MPLA is smaller than PLA's thermal degradation temperature (350 C) [79].

As shown in Figure 11 and Table 4, the Cu-PLA specimens degrade in the approximate temperature range of 300 to 400 C and with residue weight percentage of 87%. The Br-PLA specimens degrade in the approximate temperature range of 240 to 310 C and with residue weight percentage of 85%. The Al-PLA specimens degrade in the approximate temperature range of 270 to 280 C and with residue weight percentage of 60.5%. The SS-

PLA specimens degrade in the approximate temperature range of 230 to 250 C and with residue weight percentage of 83.5%. The HC-PLA specimens degrade in the approximate temperature range of 260 to 270 C and with residue weight percentage of 76%.

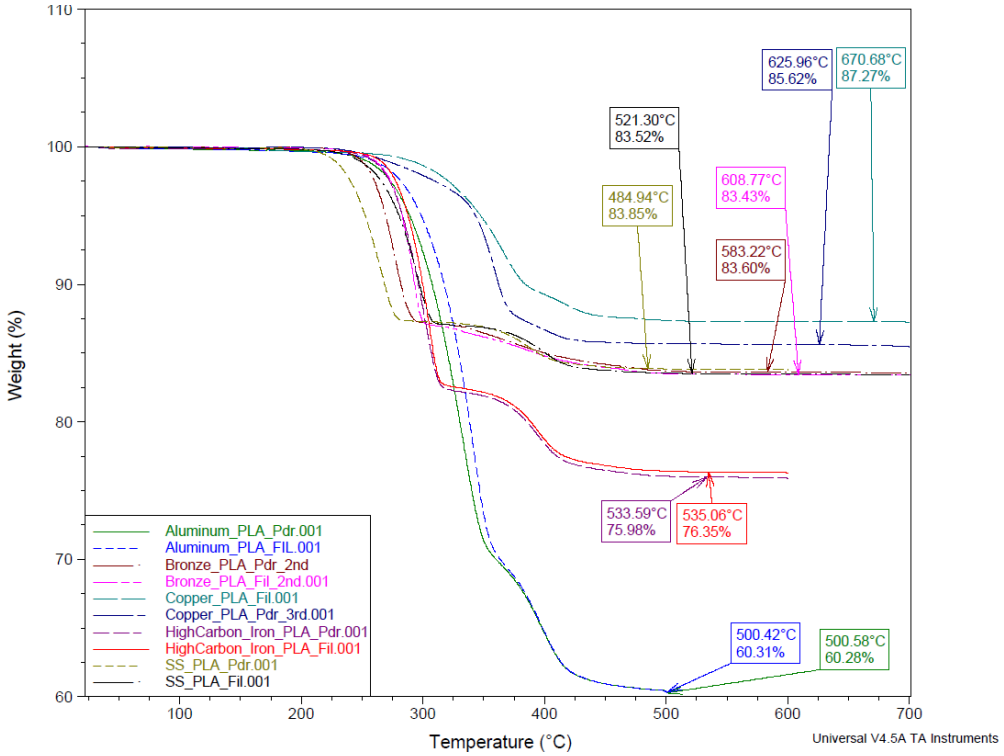

Figure 11: Temperature vs. weight plot for all the MPLA in powder or chunk form

Table 4: The thermal degradation temperature of each MPLA

Material	Thermal Degradation Starting Temperature (C)	Fully Degradation Temperature (C)	Weight %
Cu-PLA	300.87	437.45	87.28
	293.73	399.49	85.51
Br-PLA	311..21	405.59	85.98
	242.52	439.45	83.60
Al-PLA	279.41	420.54	60.49
	271.37	420.65	60.45
SS-PLA	252.08	424.64	83.44
	227.33	408.27	83.80
HC-PLA	267.83	422.10	75.96
	262.95	420.65	76.36

3.2.2. Thermomechanical Analysis (TMA)

Figure 12 shows the thermomechanical tester, TMA Q Series 400, used in this study. TMA measures the material deformation under the controlled thermal conditions. The objective of the TMA test is to study the coefficient of thermal expansion (CTE) of fabricated products. The specimens studied were made of Cu, Al, HC, and PLA. Specimens are cubes with a side length of 7 mm and fabricated with 0.1 mm layer height and contour infill pattern.

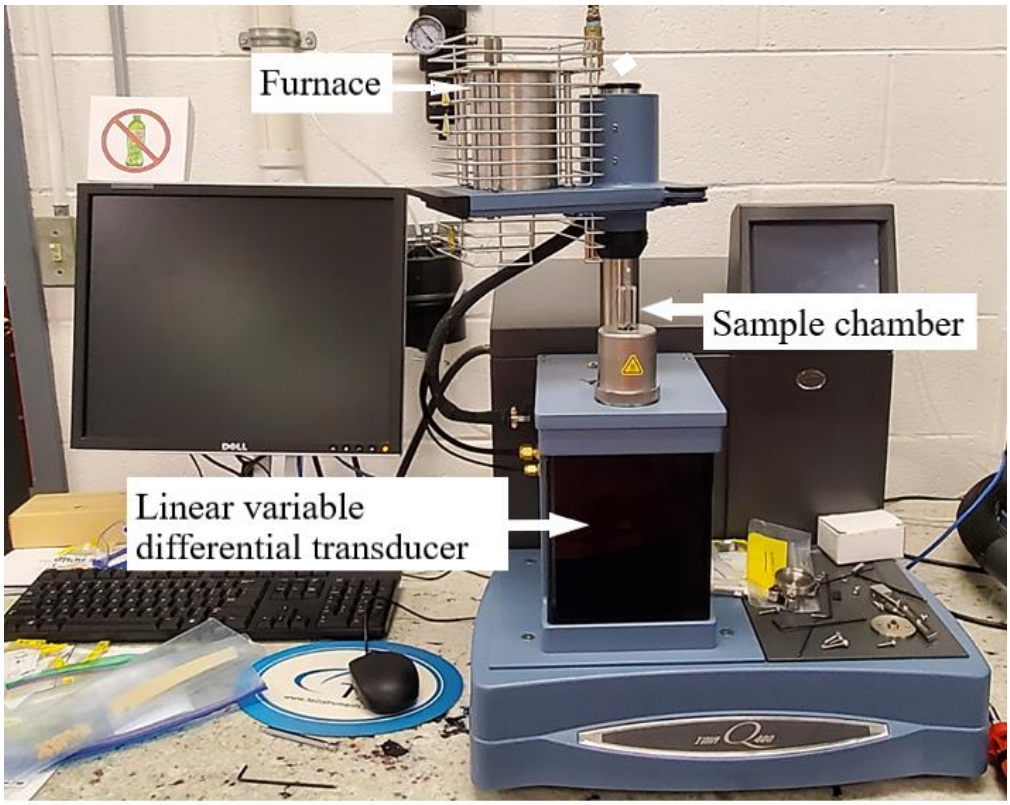

Figure 12: Thermo-mechanical analysis tester (TMA Q400)

3.2.2.1. Test Procedure and Parameter Settings

The specimen in the form of a cube is loaded into the machine by placing it on a quartz stage, close to the thermocouple. A flat-tipped standard expansion probe is placed on the specimen to apply a static force of 0.05 N. The test was carried out in a controlled environment. The Helium gas with a rate of 50 mL/min was used as the purge gas in the test process. The maximum temperature used for the test was set at 45 C, which is lower than the glass transition temperature of PLA with 60 C. This prevents the specimens' deformation by the probe and causing incorrect data under high-temperature conditions. For data accuracy, according to the ASTM standard, the temperature difference needs to be in the range of 50-100 C [80]. So, the specimens need to be cooled before the start of the test. Nitrogen was used to reach the desired negative temperature with a rate of 50 mL/min. After the test is started, the temperature was increased to 45 C with a rate of 5 C/min.

3.2.2.2. TMA Result

Figure 13 shows the change in the dimension of the samples at different temperatures. As shown, all four plots of data have curvature at the beginning of the plot which is because of purging the nitrogen gas into the chamber.

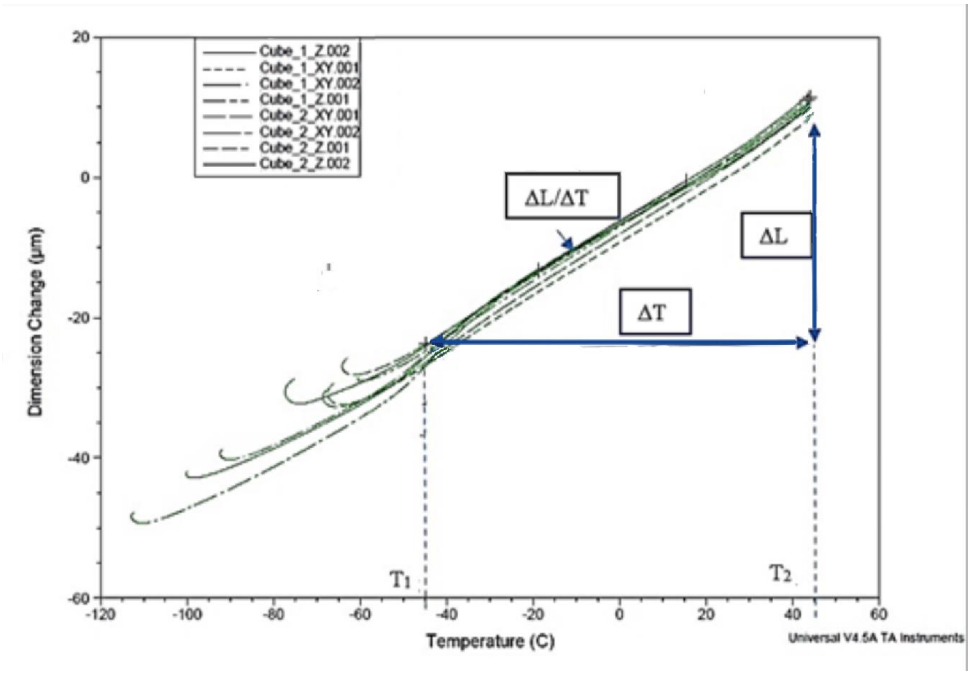

Figure 13: TMA plot for Bronze filament

The CTE of the specimen can be calculated using equation 1.

$$\alpha_m = \frac{\Delta L_{Sp}}{L \times \Delta T} \quad (1)$$

where:

α_m = mean coefficient of linear thermal expansion, µm/(m·C),

ΔL_{Sp} = dimension change, µm,

ΔT = temperature difference over which the dimension change is measured, C,

L = specimen length at room temperature, m.

Table 5 shows the average CTE of all four specimens with different testing directions and in the temperature range of -50 to 40 C.

Table 5: CTE of different filaments in the different printing directions

Material	Average CTE mm/ (m C)		Metal Weight %
	X/Y direction	Z direction	
PLA	0.07906	0.07983	0
Copper PLA	0.05646	0.06311	90
Aluminum PLA	0.06927	0.07244	65
High Carbon Iron PLA	0.06413	0.06980	80

Figure 14 demonstrates the CTE value for all four specimens. The tests were conducted in two different testing directions of the Z-axis and X/Y axis of the specimens. As shown in Figure 14, all of the MPLA specimens have a smaller CTE value than PLA specimens' CTE value. CTE value for MPLA specimens is much larger than typical metals [81]. The idea of sintering is to use the thermal expansion of the metal powder to push out the air in the structure and to form a solid part. Because the CTE of PLA is larger than metal, the expansion of the PLA in the filament material dominates the expansion of the metal. So, it will create a larger void space between the metal particles.

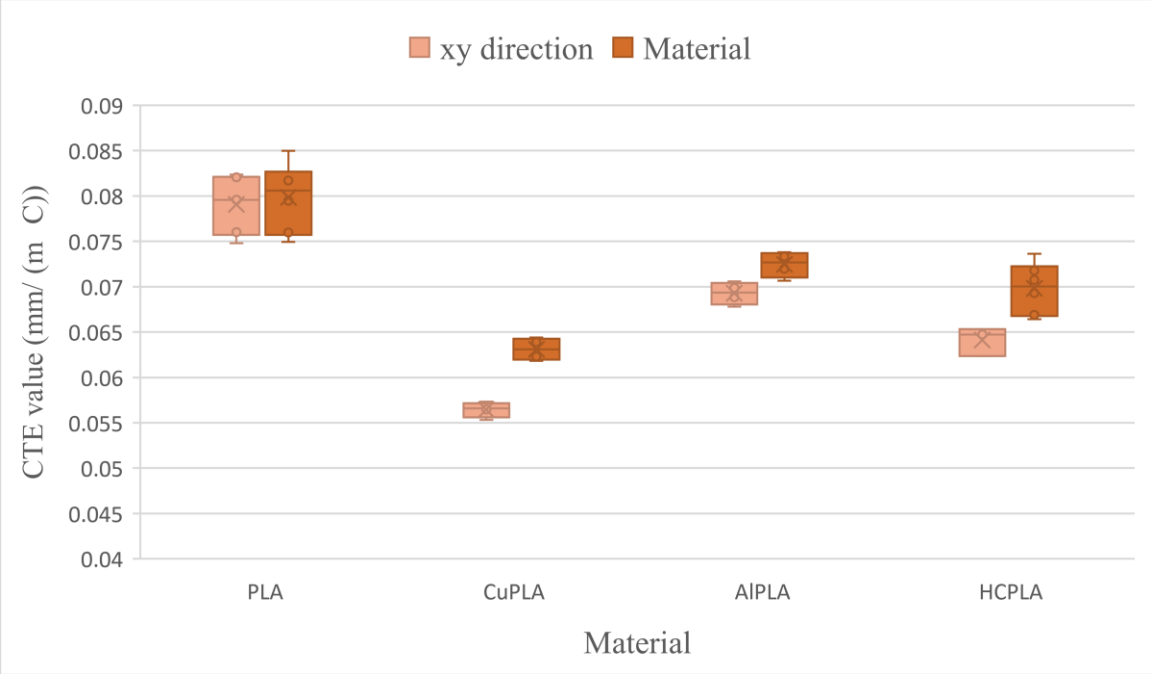

Figure 14: Variation in the CTE values of MPLA with difference test direction

As can be seen, CTE of PLA in the X/Y and Z direction equals 0.07906 mm/(m·C) and 0.07983 mm/(m·C), respectively. The result shows that the CTE of MPLA in Z direction is higher than X/Y-direction. CTE of Al-PLA in the X/Y and Z-direction equals 0.0627 mm/(m·C) and 0.07244 mm/(m·C), respectively. CTE of Cu-PLA in the X/Y and Z- direction equals 0.05646 mm/(m·C) and 0.06311 mm/(m·C), respectively. CTE of HC-PLA in the X/Y and Z-direction equals 0.06413 mm/(m·C) and 0.06890 mm/(m·C), respectively. So, the CTE value for HC-PLA and Al-PLA is almost in the same range and higher than Cu-PLA. It can be seen in Figure14 that the CTE values of Z-direction specimens are higher than X/Y- direction. This may be caused by the number of layers in the testing direction. The layer number count in Z-direction is approximate of 69 and the layer number count in X/Y- direction is approximate 8. This indicates that CTE of specimens increase as the number of layer increases.

3.4. Mechanical Analysis

In order to study the behavior of metal-based 3D printed parts in compression and tensile loading, compression and tensile tests were conducted.

3.4.1. Compression Test

The testing machine used in this study is GEOTAC with the Sigma-1 automated load test system and 2000 lb load-cell. The specimens' dimensions are shown in Figure 15, which is one of the ASTM suggested for solid cylindrical specimens with L/D ratio of two. Cu-PLA, Br-PLA, Al-PLA, HC-PLA, and regular PLA filaments were used to fabricate the specimens. Each material has been tested for a minimum number of four times. The specimen was placed at the center of the lower platen which was below the loading piston. By following the ASTM standard, the test was performed with a speed of 0.005 in./in./min. with a maximum strain limit of 40%.

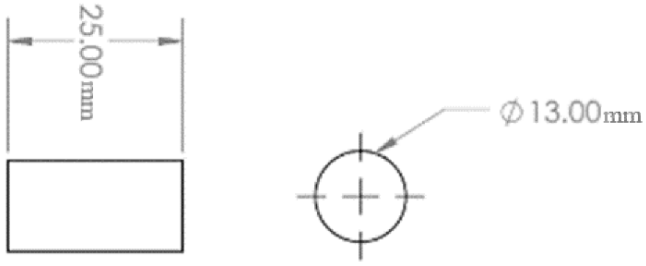

Figure 15: ASTM E9-19 short solid cylindrical specimens [82]

3.4.1.1. Compression test results

The result of compression tests was presented as stress-strain curves which are shown in Figure 16 to 20. As presented in these figures, the PLA has the highest compression stress compared with all other MPLA materials. As shown in Table 6, the compressive stress of the MPLA specimen is in the range of 20-35 MPa, while these values for PLA specimen are in the range of 58-62 MPa. Comparing the compression behavior of the MPLA and PLA specimens show that the metal powder in the PLA is weakening the mechanical properties of the product.

Figure 16 shows the compression test results of Br-PLA.

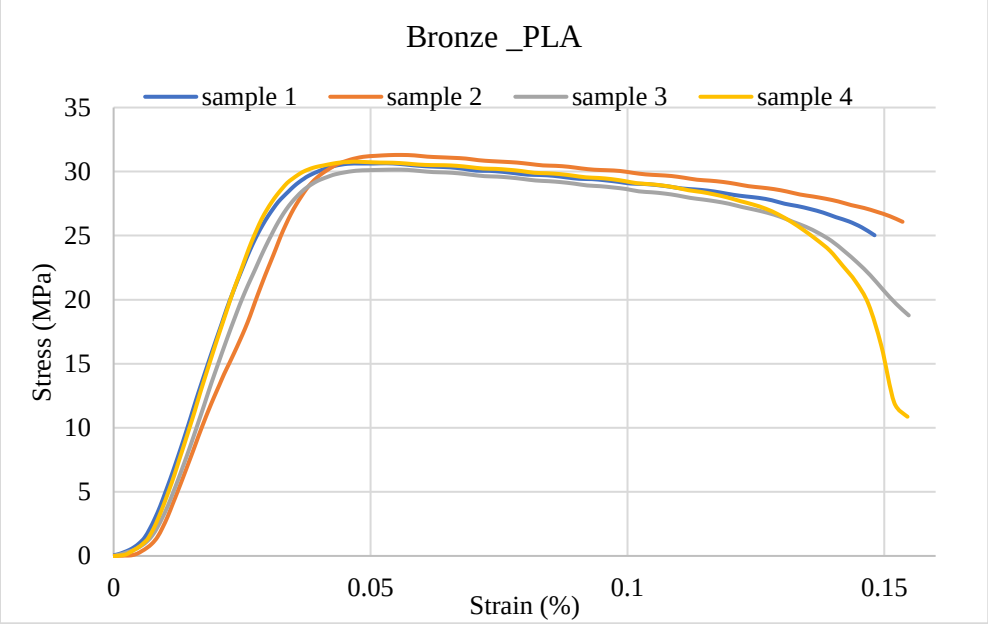

Figure 16: Stress-strain curve for Br-PLA after performing compression testing

Figure 17 shows the compression test results of HC-PLA.

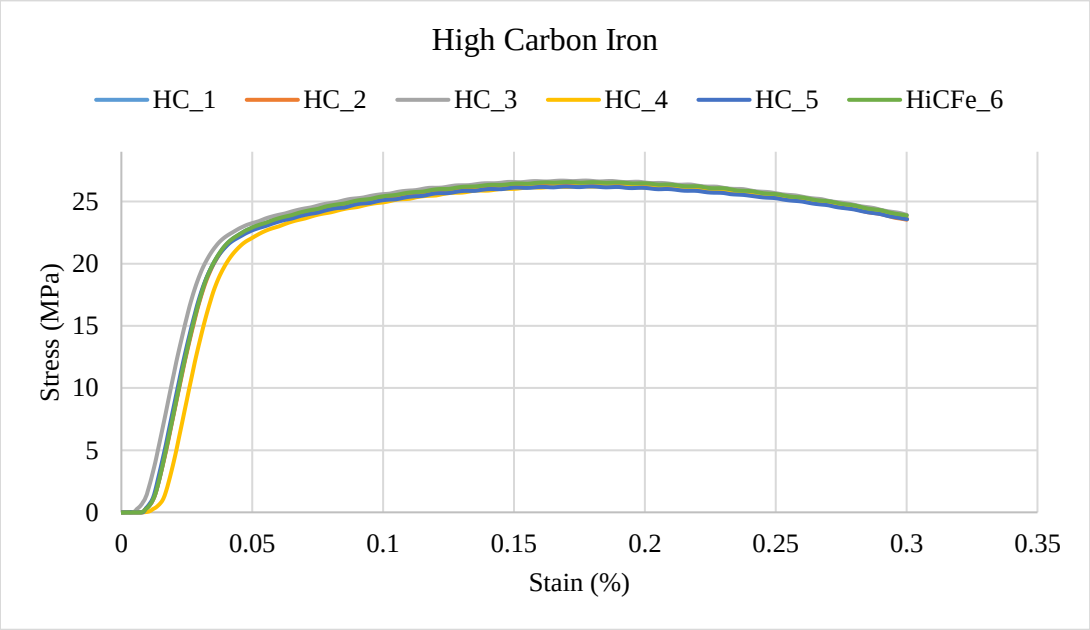

Figure 17: Stress-strain curve for HC-PLA after performing compression testing

Figure 18 shows the compression test results of Al-PLA.

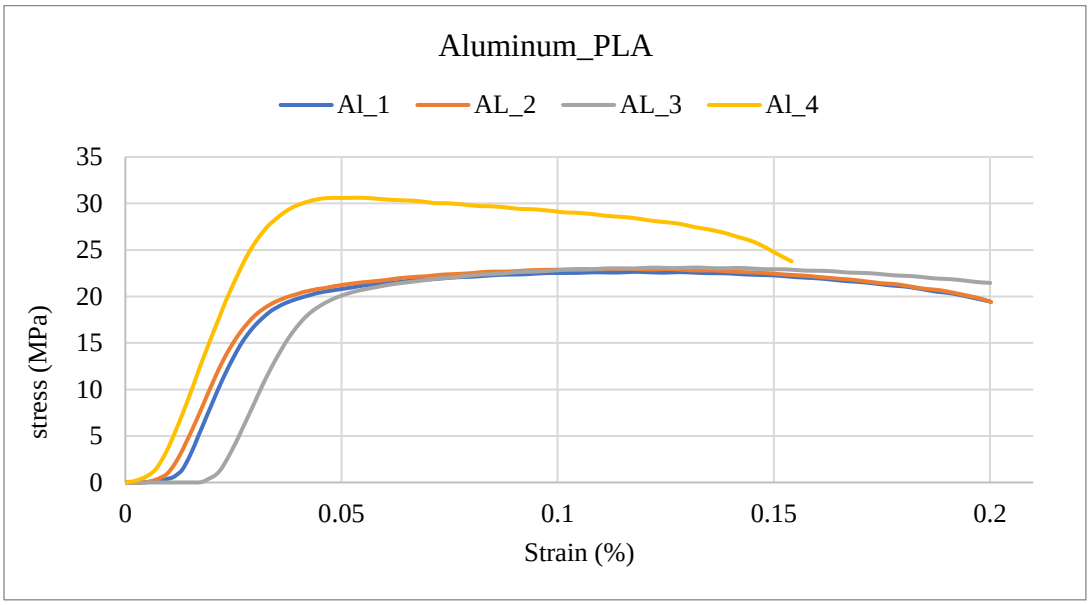

Figure 18: Stress-strain curve for Al-PLA after performing compression testing

Figure 19 shows the compression test results of Al-PLA.

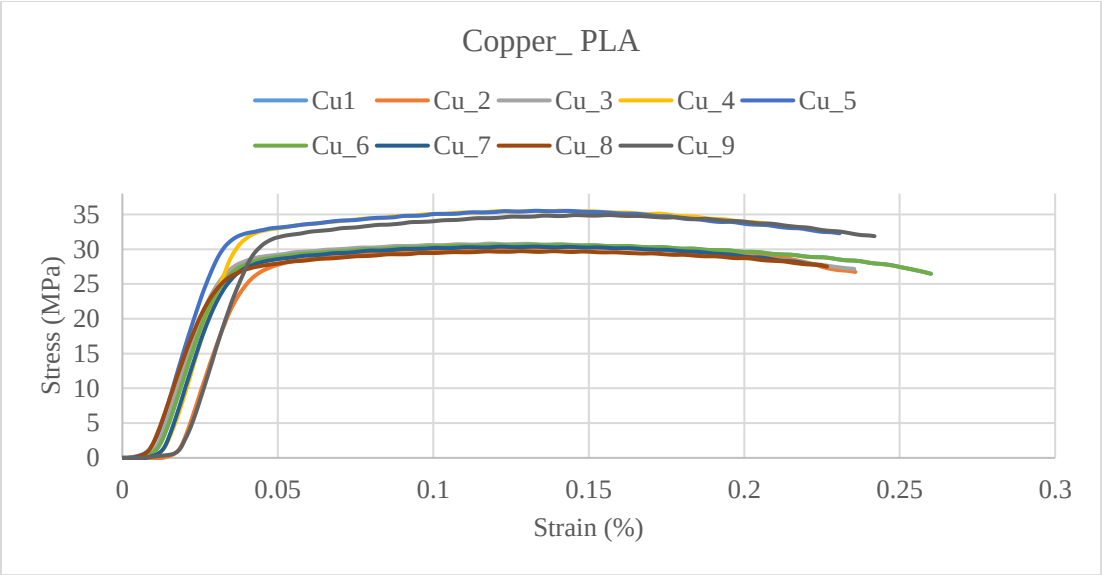

Figure 19: Stress-strain curve for Cu-PLA after performing compression testing

Figure 20 shows the compression test results of PLA.

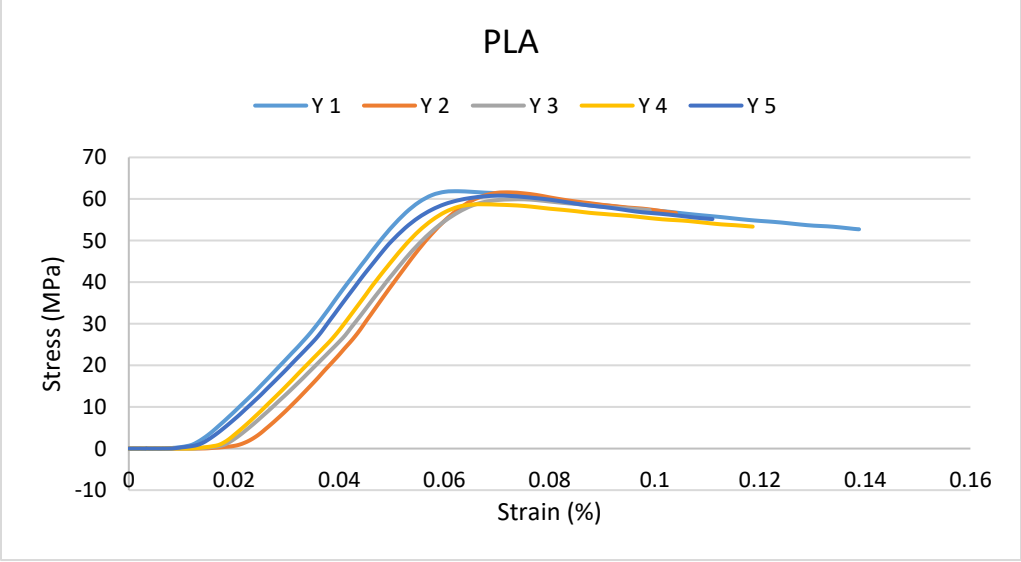

Figure 20: Strain-stress curve of PLA after performing compression testing

Table 6: Compressive properties of MPLA and PLA materials

Material	Compressive Strength (MPa)	Modulus of Elasticity (MPa)	Yield Strength (MPa)
Cu-PLA	30.64798	1386.631	24
	30.31403	1325.075	22.7
	30.80277	1393.562	24.7
	35.54069	1461.35	30.4
	35.53056	1469.259	30.1
	35.19999	1455.491	24
	30.37529	1378.15	23.8
	29.71934	1283.671	22
	34.90537	1416.271	29
Al-PLA	22.64728	1100.876	16.8
	22.97757	1061.923	17
	23.10618	1001.737	17.2
	30.61576	1246.187	26
Br-PLA	30.64836	1247.474	26
	31.29781	1059.806	28
	30.15199	1188.056	25.4

Table 6 (Continued)

Material	Compressive Strength (MPa)	Modulus of Elasticity (MPa)	Yield Strength (MPa)
Br-PLA	30.77698	1286.767	27.2
HC-PLA	26.56692	1027.291	18.9
	26.42708	1021.008	18.7
	26.68386	1023.344	18.8
	26.25037	1012.892	18.2
	26.21146	1015.524	18.4
	28.04996	960.045	19.6
PLA	61.86673	1748.881	59
	61.58551	1789.584	57
	59.92481	1661.038	55
	58.72637	1723.191	55
	60.81187	1722.052	55

3.5.2. Tensile Test

The tensile properties of MPLA specimens were studied and the effect of printing parameters including material type, layer thickness, and sintering temperature on UTS and E were investigated. Unsintered MPLA specimens were printed with a layer height of 0.1 mm. The sintered Cu-PLA specimens were printed with layer thicknesses of 0.1, 0.2, and 0.3 mm and sintering temperatures of 1050 and 1065 C.

The testing machine used for the tensile test is the Instron 5582 universal testing machine shown in Figure 21. The testing machine can collect and analyze the data through BLUEHILL software tool.

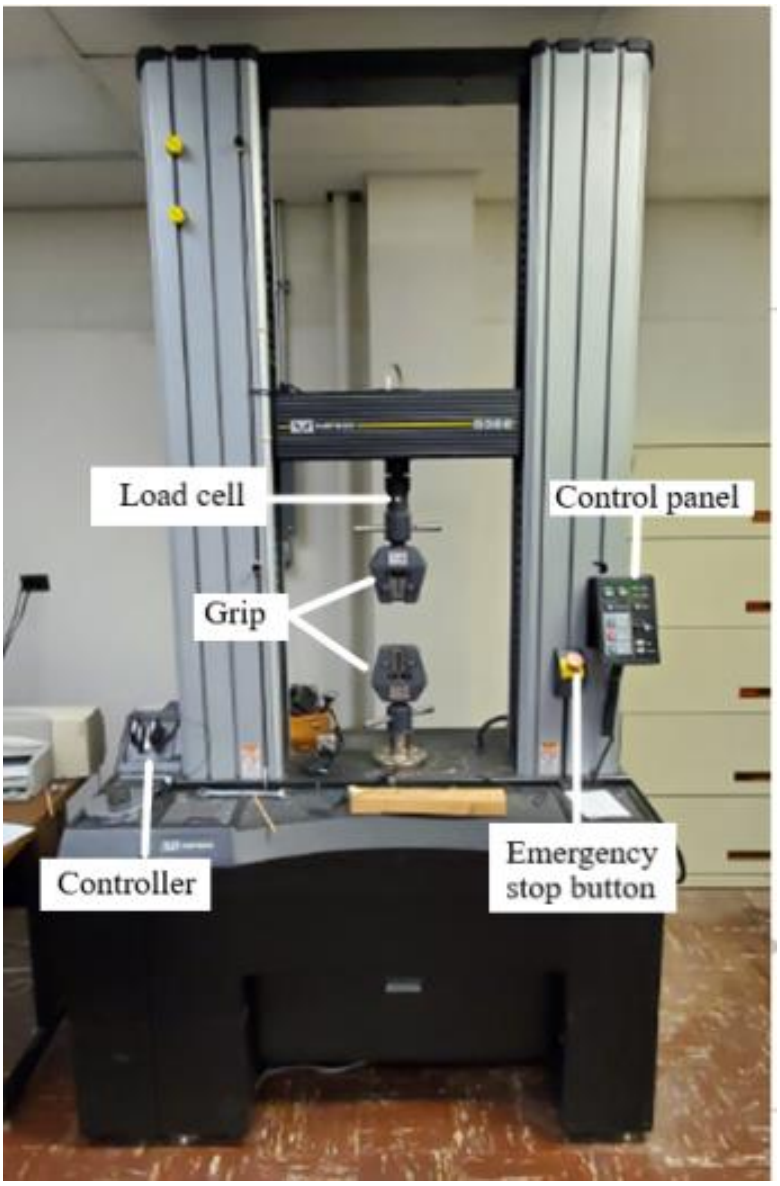

Figure 21: Instron 5582 universal testing machine

The unsintered tensile specimens are made of Cu-PLA, Al-PLA, HC-PLA, and regular PLA filaments. All the specimens are produced according to the ASTM standard D638 type V. Figure 22 demonstrates dimensions of the tensile specimen.

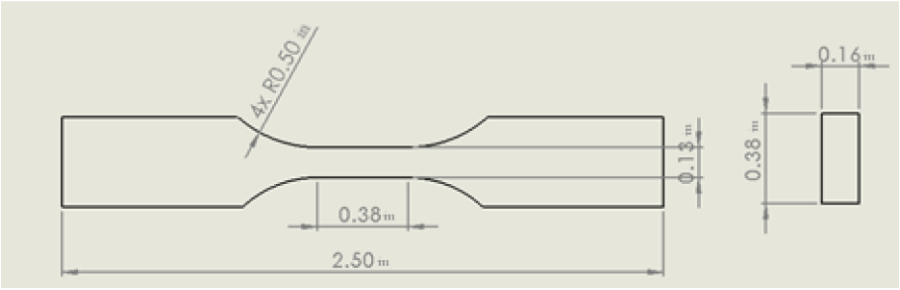

Figure 22: ASTM D638 type V model for tensile test

The printing parameters used for printing the unsintered tensile specimens are shown in table 7. The flow rate varies depending on the filament's type.

The sintered tensile specimens were printed according to the ASTM E8E8M for the tensile test of Powder Metallurgy (PM) specimens. Figure 23 shows the dimension of the sintered tensile specimen. This tensile specimen was fabricated using Cu-PLA filaments and sintered by the Lindberg Blue M furnace. For sintered specimens, the layer thickness

Table 7: Fixed controllable settings for the unsintered specimen.

Control Settings	The parameters of printing
Base Material	PLA
Supports	No supports
Skirt Line Count	3
Infill Density	100%
Wall layers	Maximum
Flow rate	110% to 130%
Roof and Floor Layers	0.4mm
Printing Temperature	230 C
Build Plate Temperature	60C
Printing Speed	10 mm/s

of 0.1, 0.2, and 0.3 mm was used. The 0.2 mm is the printer's default layer thickness, 0.3 mm is the most commonly used layer thickness based on the nozzle size, and 0.1 mm is the minimum layer height the printer can print without nozzle clogging and nozzle abrasion.

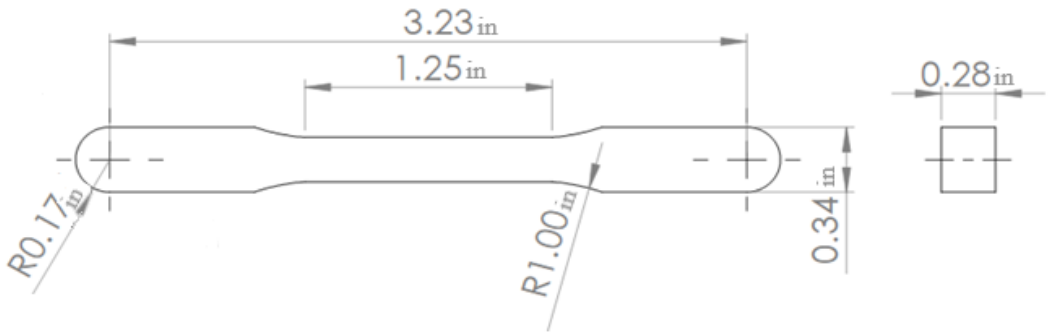

Figure 23: ASTM E8E8M PM tensile model for tensile test

Figure 24 demonstrates the grip, extensometer, and the sintered specimen during the tensile test. The test speed for sintered MPLA specimens was 0.3 mm/mm/min. The test speed for unsintered MPLA specimens was 5 mm/min.

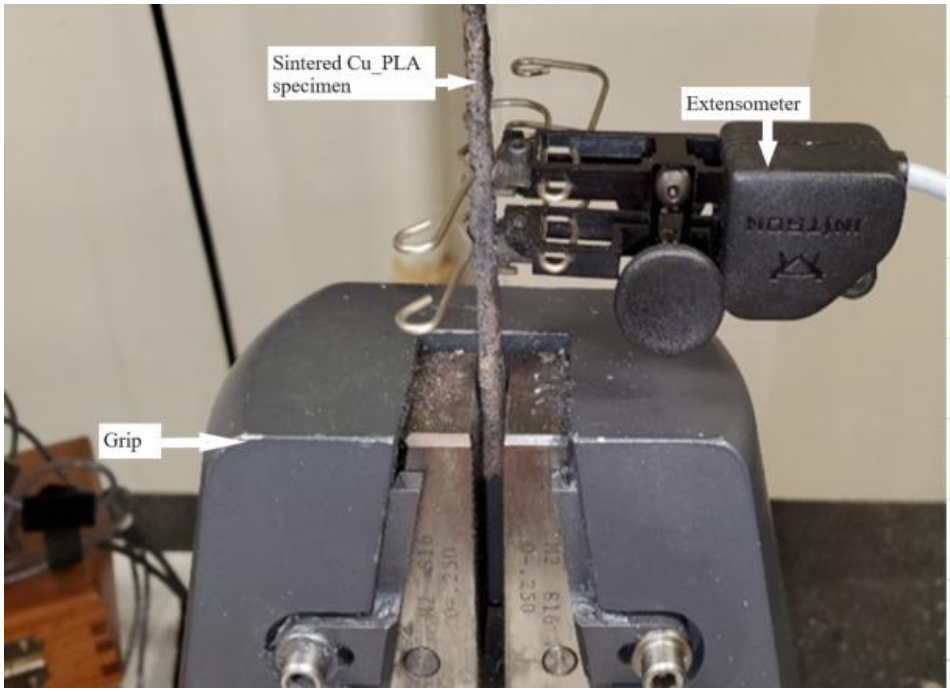

Figure 24: Specimen installed with the extensometer

3.5.3. Tensile Test Results

Table 8 shows the UTS, yield stress, and E results for the unsintered specimens. As shown, the UTS values for the unsintered MPLA specimens are significantly lower than the UTS values of PLA specimens. As can be seen in the table, the E of all specimens is in a similar range, while the UTS and yield strength of MPLA specimens are lower than PLA specimens.

Table 8: Tensile test result for unsintered specimens

	Sample #	Ultimate Tensile Strength (MPa)	Yield Stress (MPa)	Young's Modulus (GPa)
PLA	1	67.0	48.5	1.2
	2	66.8	48.0	1.1
	3	66.8	46.0	1.1
Cu-PLA	1	12.5	10.1	0.8
	2	22.3	18.2	1.4
	3	22.1	18.1	1.4
	4	22.8	18.7	1.4
HC-PLA	1	19.3	16.0	1.1
	2	18.6	15.8	1.2
Al-PLA	1	19.8	16.0	1.2
	2	20.9	17.1	1.2
	3	19.2	17.0	1.2

Figure 25 shows the strain-stress curve of Cu-PLA specimens sintered at 1050 C. Tensile properties shown in Table 9 were attained by analysis of the curve. The test has been repeated two times. Comparing the Tables 8 and 9 shows that the sintering process has a considerable effect on the UTS of Cu-PLA specimens.

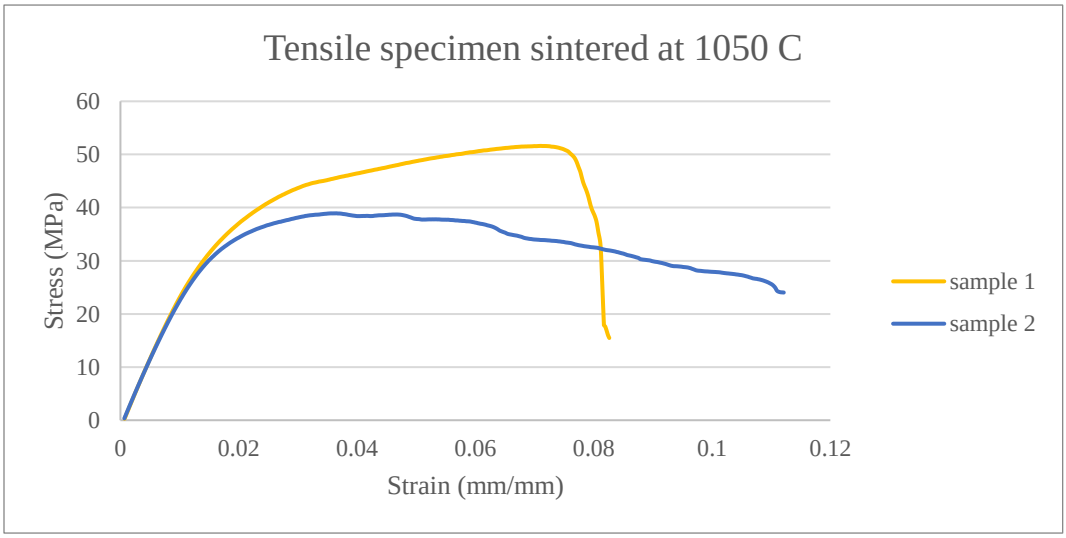

Figure 25: Strain-Stress curve of low-temperature sintered specimens

Table 9: Tensile property of Cu-PLA sintered at 1050 C

	Layer Height (mm)	Ultimate Tensile Strength (MPa)	E (GPa)	Yield Strength (MPa)
Sintered at 1050 C	0.1	51.6	2.95	21
	0.1	38.9	2.92	20.1

The results show that increasing the sintering temperature, while holding the layer thickness at constant value (0.1 mm), increase the tensile strength. It can be observed that low sintering temperature does not create significantly improve on tensile properties and analysis of mechanical properties will be proceeded on higher sintering temperatures.

Figure 26 shows the stress-strain plot of the specimens sintered under 1065 C. Also, Table 10 shows the tensile properties of the Cu-PLA specimens sintered at 1065 C. As the results show, sintering at higher temperatures improves the mechanical performance of the specimens including UTS, Yield stress, and E. Comparing the results with previous tables and the plots show that the specimen's UTS is greatly improved after the sintering process. The UTS of sintered Cu-PLA specimens is about five to eight times of the UTS of the unsintered Cu-PLA specimens. Moreover, E of the sintered specimen has improved nearly 30 times compared with the unsintered specimen.

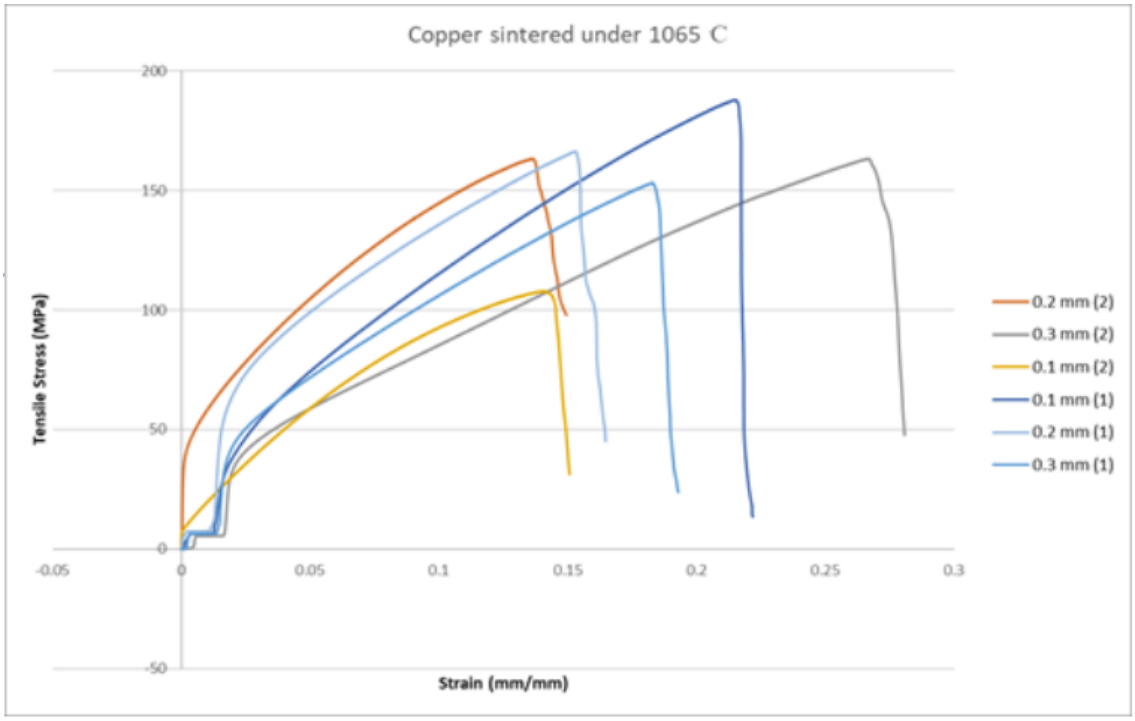

Figure 26: Strain-Stress Plot of Copper Sintered at 1065C

Table 10: Sintered Copper-PLA specimen tensile properties

	Layer Height mm	**Ultimate Tensile Strength MPa**	**Yield Stress MPa**	**E GPa**
Sintered at 1065 C	0.1	187.99	51	101
	0.1	108	10	82
	0.2	166	36	39
	0.2	163	44	48
	0.3	153	39	15
	0.3	163	36	13

Table 11 compares the mechanical properties of MME specimens with metallic and polymeric materials manufactured with traditional methods, and other AM technologies. It can be seen from the table that the before sintering the MPLA does not have proper mechanical performance. However, after sintering process, the mechanical performance of the MME copper specimen can reach 89% of conventional annealed copper tensile strength [81]. The mechanical properties of MME is a bit lower than the traditionally produced Cu parts, but it still has a higher mechanical property compared with SLM, EBM, and Jet Binder produced parts.

Table 11: The current material and MME mechanical properties

	UTS (MPa)	**E (GPa)**	**Yield Stress (MPa)**
MME Copper	108-188	13-101	10-51
Indirect SLM Copper	8 [83]	NA	NA
Direct SLM Copper	149 [84]	NA	NA
EBM Copper [85]	177	NA	87
Jet Binder Copper	176.35 [86]	NA	NA
Copper (Annealed) [81]	210	110	33.3
SLM SS 316L [71]	648	320	541
FDM SS 316L [71]	465	152	167
Unsintered Cu-PLA	22.3	1.4	18.2
PLA	66.8	48.0	1.1
Nylon	19.17	0.297	103
Nylon-Carbon Fiber [87][88]	446.87	51.4	NA

CHAPTER 4: DESIGN OF EXPERIMENTS

In this chapter, an experimental design was implemented on the tensile test results. The analysis was performed to investigate the influence of the input parameters of sintering temperature and layer height and their interactions on the mechanical properties of tensile strength and Young's modulus. In this study, a two-way ANOVA model with interaction was utilized. The equation 2 demonstrates the ANOVA model is given below [89]:

$$Y_{ij} = \mu_{..} + \alpha_i + \beta_j + (\alpha\beta)_{ij} + \varepsilon_{ij} \qquad (2)$$

where Y_{ij} is the response variable (either tensile strength or Young's modulus), $\mu_{..}$ is the overall mean, α_i is the main effect for factor A (sintering temperature) at the i-th level, β_j is the main effect for factor B (layer height) at the j-th level, and $(\alpha\beta)_{ij}$ represent the interaction effects.

4.1. ANOVA for Tensile Properties

In this section, the two-way ANOVA with interactions was applied to the response variables tensile strength for Cu-PLA with the dependent variables sintering temperature and printing layer height. In order to sinter the test specimens, 1050 C and 1065 C sintering temperatures were utilized. Also, three different levels of layer height were used to investigate the effect of layer height on tensile strength, 0.1 mm, 0.2 mm, and 0.3 mm.

4.1.2. Analysis of tensile test results

The two-way ANOVA was performed to investigate the influence of sintering temperature and layer height on tensile strength. Table 12 and 13 demonstrate the ANOVA table for UTS and Young's Modulus of sintered Cu-PLA specimens.

Table 12: ANOVA table for UTS

	Df	*SSE*	*MSE*	*F value*	*p-value*
UTS					
Factor A (layer height)	1	276.5	138.3	22.4040	0.852709
Factor B (temperature)	2	18675.7	1875.7	0.1659	0.009082
Residuals	4	3334.3	833.6		

Table 13: ANOVA table for Young's modulus

	Df	*SSE*	*MSE*	*F value*	*p-value*
Young's Modulus					
Factor A (layer height)	2	6120.3	3060.2	54.891	0.001553
Factor B (temperature)	1	3280.7	3280.7	58.846	0.001236
Residuals	4	223	55.7		

The result of tensile strength for the first group (0.1 mm layer thickness and 1050 C sintering temperature) showed 50 MPa, while the second group variables (0.1 mm layer

thickness and 1065 C sintering temperature) yielded higher strength values which is around 150 MPa.

The p-value of both factors shown in Table 13 is smaller than α value (0.05). This shows that the layer height and sintering temperature have an effect on the Young's modulus.

4.2. Linear Regression for Young's Modulus

Figure 27 shows the Young's modulus of specimens printed with different layer thicknesses. The graph shows that Young's modulus decreases as the layer height increases. The fitted linear regression model was calculated in EXCEL and linear relationship between Young's modulus and the layer height is shown.

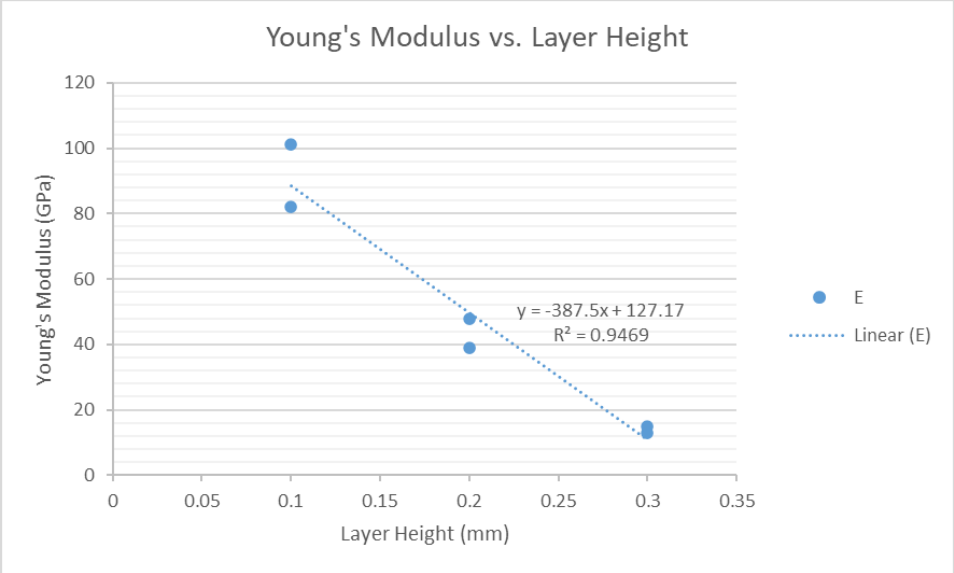

Figure 27: Plot for Young's Modulus vs Layer Height

It can be clearly seen that there is a negative correlation between Young's modulus and the layer height. The decrease in layer height increases the material stiffness properties. This is because the copper particles in the PLA filament is getting squeezed while the print head nozzle is depositing the layers on the bed platform. This results the better combining process of the copper particles which less voids are created in the specimen and ultimately increases the mechanical properties of Cu-PLA sintered specimens. Figure 28 shows how lower layer heights decreases the distance among the copper particles with respect to higher layer heights.

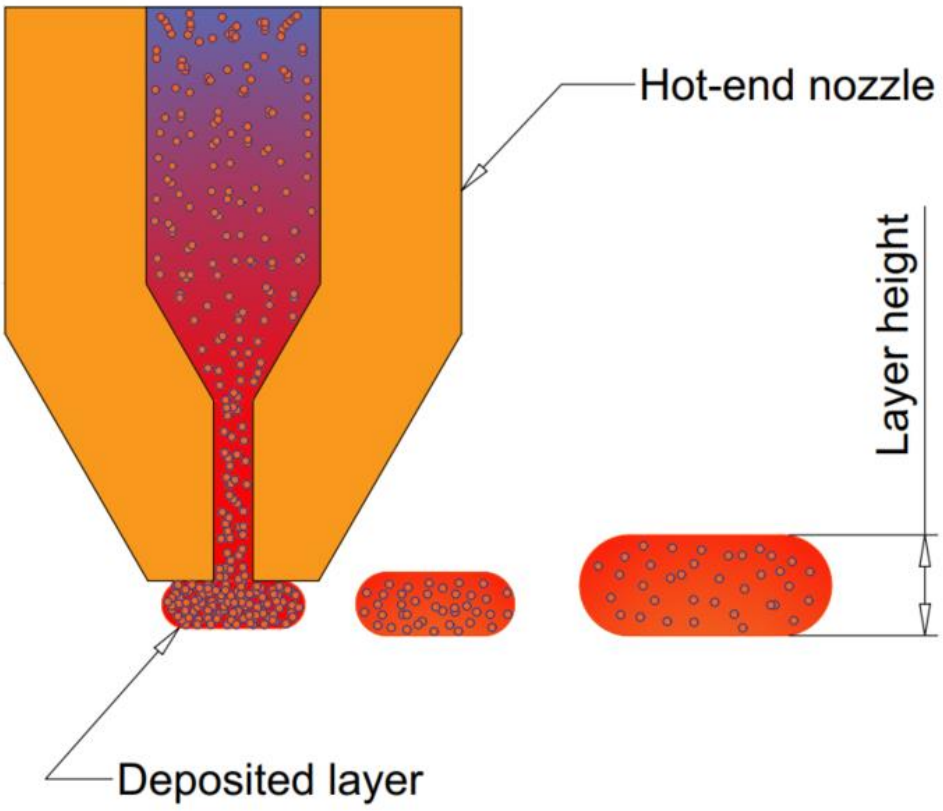

Figure 28: The effect of lower layer height on the deposited beads

4.3. Discussion

Statistical analysis was performed in order to investigate the influence of processing parameters *i.e.* sintering temperature and layer thickness on the behavior of tensile properties. ANOVA analysis concludes that sintering temperature and layer height have a significant effect on Young's modulus values. However, layer height does not influence the UTS results. Moreover, linear regression model shows that there is a negative correlation between layer height and Young's modulus *i.e.* decreasing layer height leads to increase the stiffness properties.

CHAPTER 5: MICROSTRUCTURAL ANALYSES

In this section, the microstructural analysis was conducted to study the fracture mechanism, internal morphology, voids, and printing quality of the specimens. In order to gain a better understanding of the internal structure of 3D printed parts, test specimens were examined with both optical microscope and SEM. Optical microscope provides overall information of the specimens. On the other hand, SEM provides the detailed information of the structure with more magnification and higher resolution on micron-sized level.

5.1. Optical Microscope

The optical microscopy was used to provide an overall view of the specimens' structure in the micron scale. As shown in Figure 29 the microscope used for this study is a Nikon Eclipse MA 100 Inverted Microscope equipped with Nikon-Elements Basic Research software.

Figure 29: The microscope used for this study: Nikon Eclipse MA 100

The cross-sectional views of unsintered Cu-PLA specimens are shown in Figure 30. As seen in the image, two different phases for metal and polymer are observed. A large part of the space is filled with PLA. The copper particles are seen with dark color on a background of polymers with brighter color. It can be seen that the copper particles are not very uniformly distributed in the PLA.

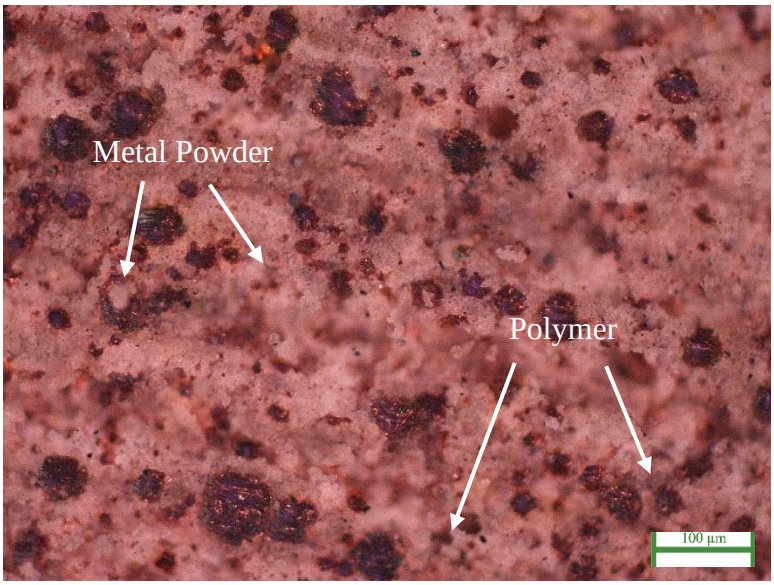

Figure 30: Unsintered Cu-PLA specimen

The cross-sectional view of the sintered Cu-PLA specimen is shown in Figure 31. After sintering, the polymer degrades and leaving behind the copper and voids as show in the Figure 31. The metal particles are fused at high temperatures, and the PLA is disappeared. The observed voids may be caused by the printing process, or it may be caused by the gas generated by the thermal decomposition of PLA during the sintering process. This is the reason that the tensile strength of the Cu-PLA is smaller than the parts produced by traditional processes. The sintering temperature is 1065 C. After cutting, the sample was polished three times. After rough grinding, alumina is used for fine polishing. The lines shown in the picture are because of the polishing process.

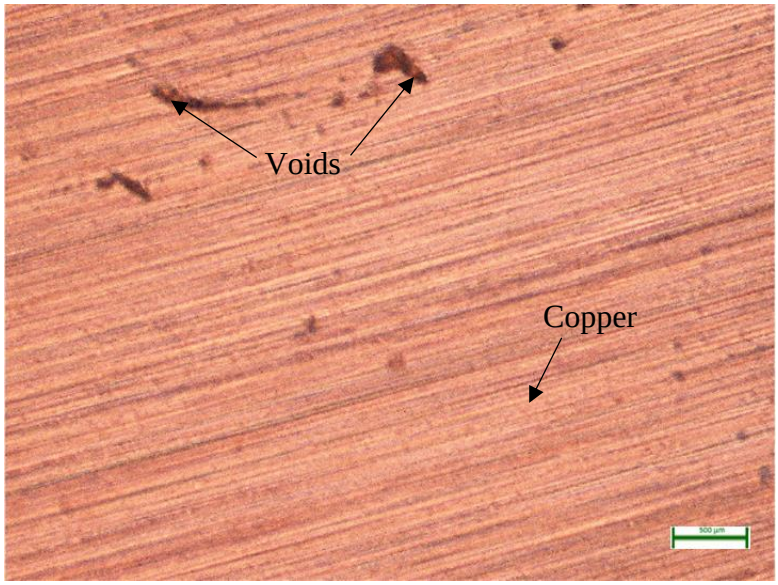

Figure 31: Sintered Cu-PLA specimen for 0.2 mm layer height

Figure 32 demonstrates the cross-sectional view of the MME specimens with two different layer heights of 0.3 mm and 0.1 mm. As can be seen, the specimen printed with 0.3 mm shows more voids than the specimen printed with 0.1 mm layer height. So, it can be concluded that, as layer height increases, the void population in the specimen increases proportionally.

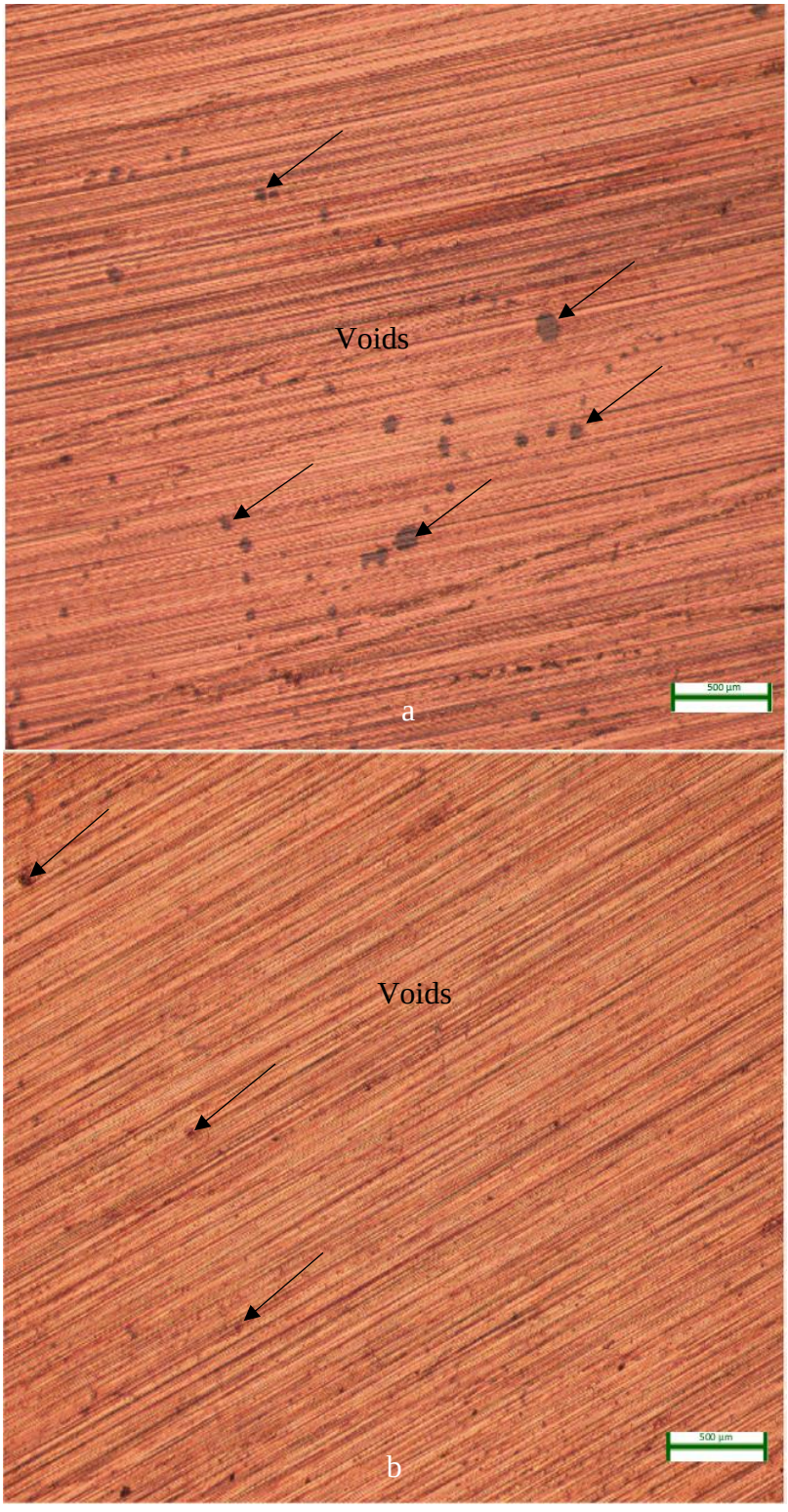

Figure 32: Sintered Cu-PLA with different layer heights: (a) 0.3mm (b) 0.1mm

Figure 33 compares the void percentage of the sintered Cu specimens at different temperatures and different layer heights. It can be seen that sintering temperature has a great influence on the void's area percentage. The average surface area changes from the initial 10.95% to 0.68%. By increasing the sintering temperature by 15 C, the void area percentage of the finished product decreases by 93.7%.

5.2. SEM

To study the details of the structure with higher magnification in nano-scale and better quality, the SEM method was used. SEM provides more details about the fracture

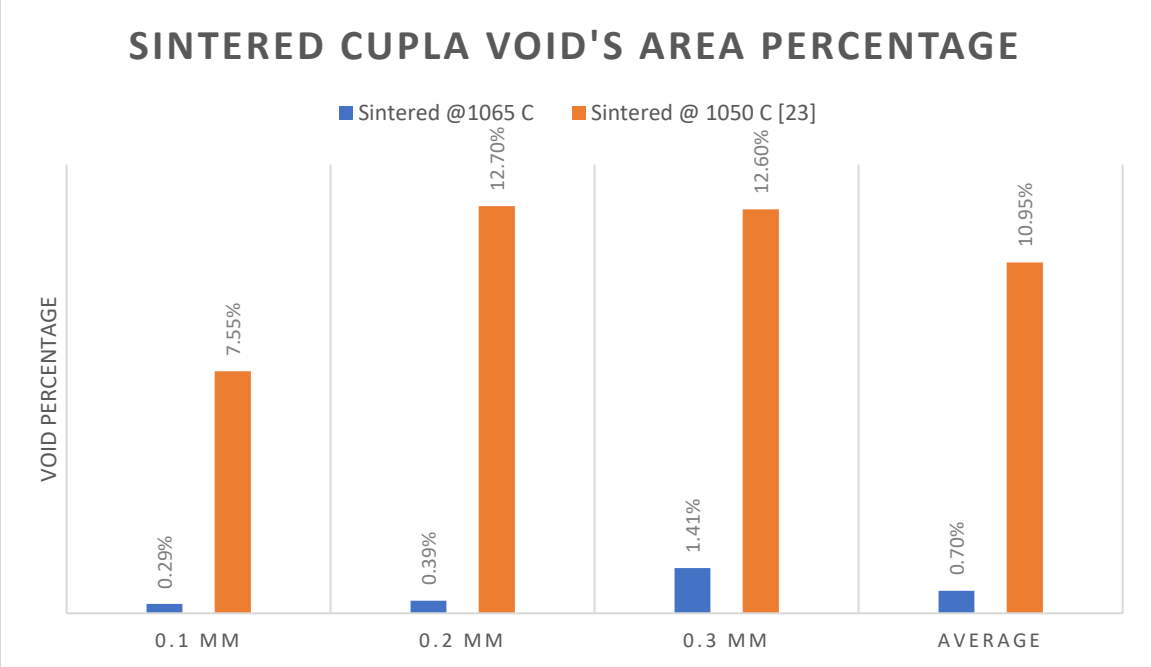

Figure 33: Void percentage of samples tested in different sintering temperature

mechanism and microstructural morphology of MPLA specimens. Figure 35 demonstrates the picture of the SEM machine.

SEM machine scans the surface of the specimen with a beam of electron. It has a couple of advantages such as high magnification, detailed view, large depth of field, and sample preparation.

Figure 35-37 shows the SEM images from the cross-section of the sintered MPA specimens with a layer height of 0.3, 0.2, and 0.1 mm, respectively. SEM test is taken from the specimens broken with the tensile test. It can be seen in the figures that the intra bead spaces (voids) decrease as the printed layer height decreases.

Figure 34: SEM machine

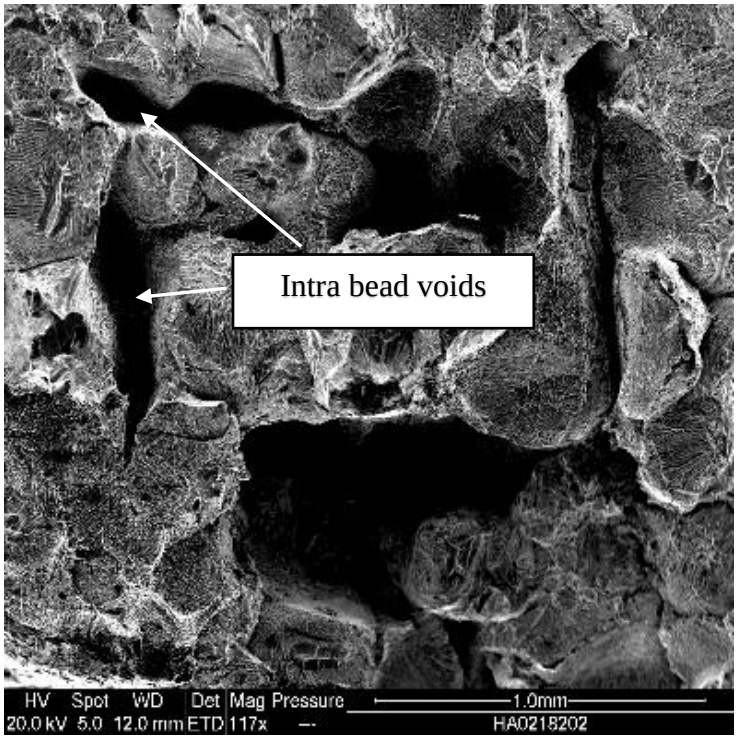

Figure 35: SEM image for sintered part 0.3mm layer height

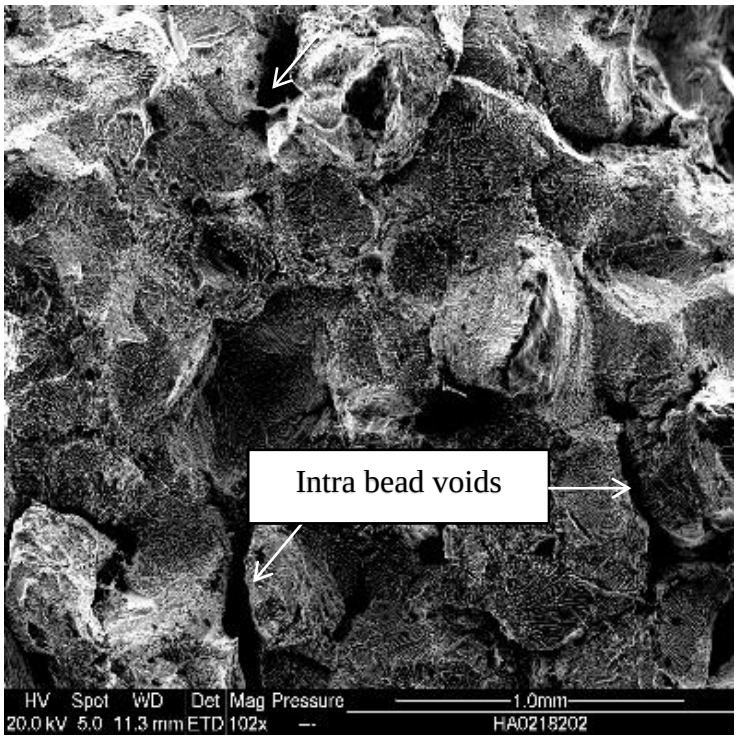

Figure 36: SEM image for sintered part 0.2mm layer height

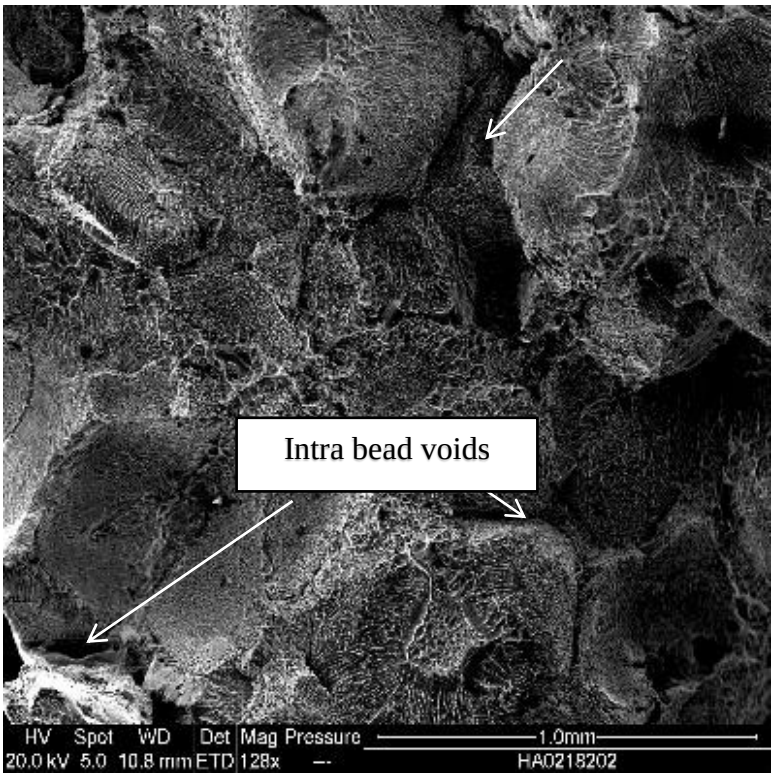

Figure 37: SEM image for sintered part 0.1mm layer height

In all of the SEM images, the fracture surfaces are not smooth and shown a lot of bright lines on the fracture surfaces. This may indicate that the tensile specimens have a ductile fracture. Figure 38 to 40 shows the fracture surfaces with larger magnification. The images show some dimples with cord distributed on the surface of fracture. As the printing layer height increases the dimples' size increases. This indicates that the ductile behaviors of the tensile specimens increase as the layer height increases. The cord shown in the dimples is typically caused by the impurity substance or second phase particles. Figure 38 to 40 shows the dimples are elongated, which indicates that during the test the force applied is not normal to the cross-section of the specimens.

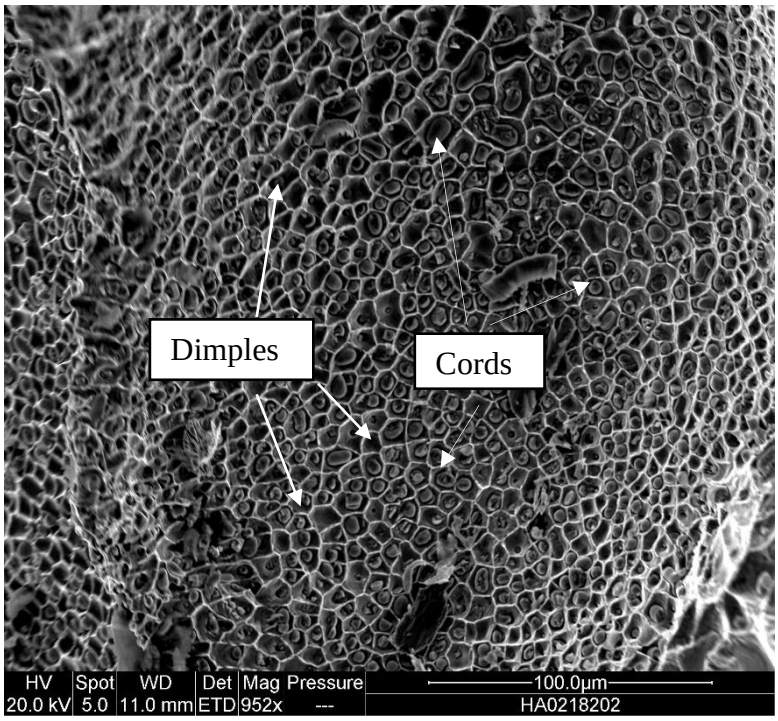

Figure 38: SEM image of sintered 0.1 mm layer height Cu-PLA tensile fracture

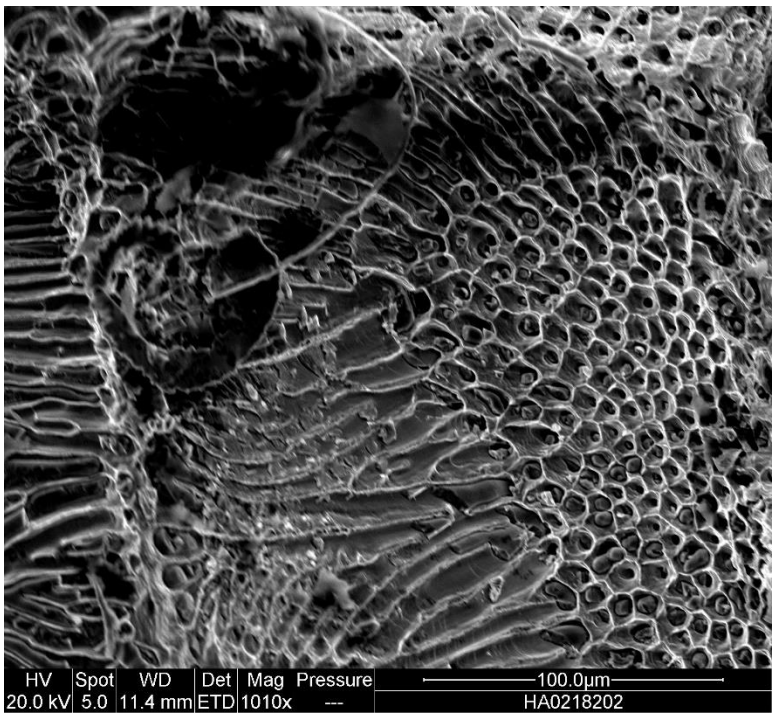

Figure 39: SEM image of sintered 0.2 mm layer height Cu-PLA tensile fracture

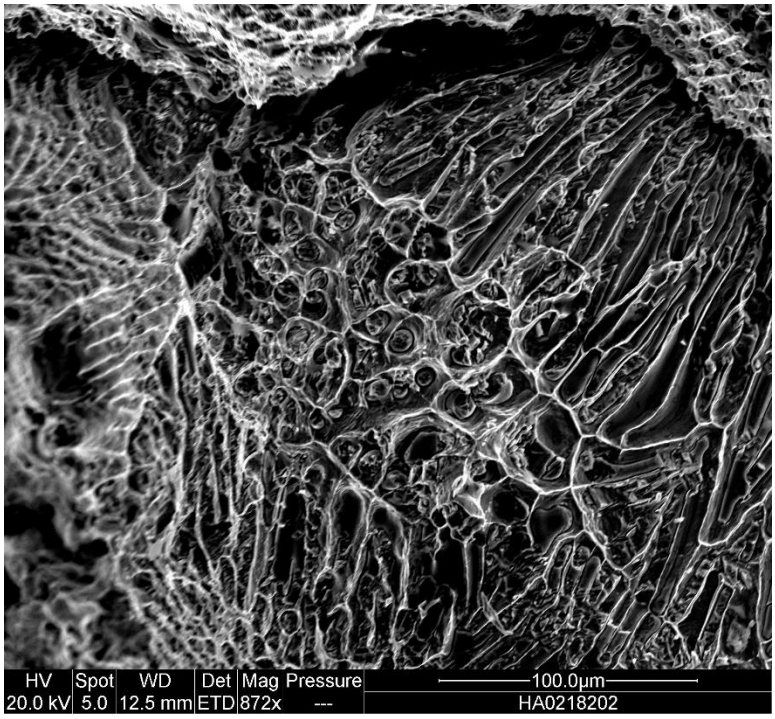

Figure 40: SEM image of sintered 0.3 mm layer height Cu-PLA tensile fracture

The SEM images demonstrate that the cell size increases as layer height increases and the sintered specimens' stress-strain plots confirm that the ductility increases as the layer height increases. As layer height increases, the void in the structure increases and the tensile test result confirms that the Young's modulus is reduced as layer height increases.

CHAPTER 6: CONCLUSION AND FUTURE WORK

The research study presented in this thesis is a unique way of manufacturing metal-based parts using low-cost MME 3D printers. Such a setup could fabricate complex and good quality metallic parts. The post processing technology used in this method is sintering. After the sintering process, the parts shrink and turns out to be metallic objects. Attributed to the porous structure, mechanical properties are not as high as those of the traditionally produced parts. Different metals (Copper, Bronze, High Carbon Steel, and Aluminum) are used in this study which are commonly used in industrial production. This preliminary investigation is original in presenting the tensile and thermal properties of MME specimens. The study shows that the tensile properties of sintered test specimen is getting closer to the regular metallic tensile specimens. It is believed that the future studies could produce higher tensile properties (close to the mechanical properties of metal). This study had to be limited to current findings reported in the thesis. Due to the COVID-19 related policies and procedures of Tennessee Tech University, it was not possible for the research team to produce enough samples to draw in-depth findings for the cases of sintered metals.

6.1. Conclusion

This research study introduced a novel method for manufacturing low-cost metal AM components. The focus of the study is to investigate the thermal and mechanical

properties of produced parts. The specimens were prepared using PLA as polymer and Cu, Al, Br, HC, and SS as a metal phase. The results of the research are summarized as follows:

- Using low-cost and easy-to-use desktop printers, metallic parts were produced successfully.
- The sintering process was conducted to improve the mechanical properties of metallic parts.
- The effect of layer height and sintering temperature on the mechanical properties of MPLA parts was studied.
- The average UTS, E, and yield strength of the unsintered MPLA specimens increase 687%, 3873%, 121% respectively after sintered at 1065 C.
- TGA study shows that the polymer compositions in the filament start the thermal degradation approximately at 300 C.
- The printing direction affects MPLA's CTE value. During the sintering process, the expansion of polymer is much larger than metal powder. So, the void is unavoidable.
- Microstructural analysis confirms that the ductility increases and E is reduced as layer height increases.
- Young's modulus is inversely proportional to layer thickness. Increasing layer height from 0.1 to 0.3 reduces E from 94.5 MPa to 43.5 MPa.
- Increasing sintering temperature from 1050 C to 1065 C increases the UTS, Yield stress, and E by 227%, 939%, 345% respectively.
- Comparing the compression behavior of the MPLA and PLA specimens shows that the metal powder in the PLA reduces the compression stress, compression modulus, and Yield Strength by 52%, 30%, 59% respectively.

6.2. Future Work

Due to the COVID-19 situation, the mechanical tests for sintered specimens were not fully completed. The low-cost MME AM method can be further advanced by improving the sintering process and enhancing the mechanical/thermal properties' database. The fatigue analysis and DMA can be made to further characterize the mechanical and thermal properties of sintered low-cost MME parts. The XRD test is needed to observe the formation of the intermetallic compounds after sintering process. While the basic mechanical/thermal properties and sintering shrinkage ratios are gradually improved, a statistical model can be created for predicting dimensional changes of parts and their mechanical properties at different sintering temperatures. Further experiments could focus on the sintering process to achieve denser parts with uniform shrinkage and enhanced mechanical properties.

REFERENCES

[1] ASTM International, “F2792-12a - Standard Terminology for Additive Manufacturing Technologies,” *Rapid Manuf. Assoc.*, pp. 10–12, 2013.

[2] K. V. Wong and A. Hernandez, “A Review of Additive Manufacturing,” *ISRN Mech. Eng.*, vol. 2012, pp. 1–10, 2012.

[3] S. Terry *et al.*, “The Influence of Smart Manufacturing towards Energy Conservation: A Review,” *Technologies*, vol. 8, no. 2, p. 31, May 2020.

[4] S.-I. Park, D. W. Rosen, S. Choi, and C. E. Duty, “Effective mechanical properties of lattice material fabricated by material extrusion additive manufacturing,” *Addit. Manuf.*, vol. 1–4, pp. 12–23, Oct. 2014.

[5] S. Meteyer, X. Xu, N. Perry, and Y. F. Zhao, “Energy and material flow analysis of binder-jetting additive manufacturing processes,” *Procedia CIRP*, vol. 15, pp. 19–25, 2014.

[6] A. Saboori, D. Gallo, S. Biamino, P. Fino, and M. Lombardi, “An overview of additive manufacturing of titanium components by directed energy deposition: Microstructure and mechanical properties,” *Appl. Sci.*, vol. 7, no. 9, 2017.

[7] A. Sauter, “TechBot: A Multimaterial Mobile 3D Printing Platform,” Tennessee tech university, 2019.

[8] Y. L. Yap, C. Wang, S. L. Sing, V. Dikshit, W. Y. Yeong, and J. Wei, “Material jetting additive manufacturing: An experimental study using designed metrological benchmarks,” *Precis. Eng.*, vol. 50, pp. 275–285, 2017.

[9] A. Gupta, M. Hussain, S. Misra, A. K. Das, and A. Mandal, “Processing and characterization of laser sintered hybrid B4C/cBN reinforced Ti-based metal matrix composite,” *Opt. Lasers Eng.*, vol. 105, no. May 2018, pp. 159–172, 2018.

[10] S. Misra, M. Hussain, A. Gupta, V. Kumar, S. Kumar, and A. K. Das, “Fabrication and characteristic evaluation of direct metal laser sintered SiC particulate reinforced Ti6Al4V metal matrix composites,” *J. Laser Appl.*, 2019.

[11] J. Park, M. J. Tari, and H. T. Hahn, “Characterization of the laminated object manufacturing (LOM) process,” *Rapid Prototyp. J.*, vol. 6, no. 1, pp. 36–50, Mar. 2000.

[12] M. Feygin and B. Hsieh, “Laminated object manufacturing: A simpler process,” *Proc. 2nd Solid Free. Fabr. Symp.*, vol. 0, pp. 123–130, 1991.

[13] M. Colopi, L. Caprio, A. G. Demir, and B. Previtali, “Selective laser melting of pure Cu with a 1 kW single mode fiber laser,” *Procedia CIRP*, vol. 74, pp. 59–63, 2018.

[14] Diptanshu, E. Young, C. Ma, S. Obeidat, B. Pang, and N. Kang, “Ceramic additive manufacturing using vat photopolymerization,” *ASME 2018 13th Int. Manuf. Sci. Eng. Conf. MSEC 2018*, vol. 1, no. October, 2018.

[15] terry Wohlers and T. Gornet, “History of additive manufacturing,” *Wohlers Rep. 2012*, pp. 32–42, 2015.

[16] R. A. Sobieszek, “Sculpture as the Sum of its Profiles: François Willème and Photosculpture in France, 1859–1868,” *Art Bull.*, vol. 62, no. 4, pp. 617–630, Dec. 1980.

[17] J. E. Blanther, “Manufacture of contour relief maps,” 1892.

[18] H. Kodama, “Stereoscopic figure drawing device,” 1980.

[19] C. W. Hull, “Apparatus for Production of Three-Dmensonal Objects By Stereo Thography,” *Patent*, no. 19, p. 16, 1984.

[20] H. Narasaki, K. Ogawa, and K. Tsujimoto, “Determination of trace phosphorus in organic materials by a combined low temperature ashing-spectrophotometry,” 1979.

[21] A. Bowyer, “3D Printing and Humanity’s First Imperfect Replicator,” *3D Print. Addit. Manuf.*, vol. 1, no. 1, pp. 4–5, Mar. 2014.

[22] M. Chinthavali, “3D Printing Technology for Food,” 2016.

[23] M. Whitaker, “The history of 3D printing in healthcare,” *Bull. R. Coll. Surg. Engl.*, vol. 96, no. 7, pp. 228–229, Jul. 2014.

[24] A. Shamir, *Computational tools for 3D printing*. 2016.

[25] D. Freeman, “Israeli scientists create world’s first 3D-printed heart using human cells,” *nbcnews*, 2019.

[26] C. Buchanan and L. Gardner, “Metal 3D printing in construction: A review of methods, research, applications, opportunities and challenges,” *Eng. Struct.*, vol. 180, no. March 2018, pp. 332–348, 2019.

[27] A. R. Mashhadi, B. Esmaeilian, and S. Behdad, “IMPACT OF ADDITIVE MANUFACTURING ADOPTION ON FUTURE OF SUPPLY CHAINS,” no. July, 2015.

[28] B. Durakovic, “Design for additive manufacturing: Benefits, trends and challenges,” *Period. Eng. Nat. Sci.*, vol. 6, no. 2, pp. 179–191, 2018.

[29] I. Fidan *et al.*, “The trends and challenges of fiber reinforced additive manufacturing,” *Int. J. Adv. Manuf. Technol.*, vol. 102, no. 5–8, pp. 1801–1818, Jun. 2019.

[30] A. Gupta, S. Hasanov, and I. Fidan, “Processing and Characterization of 3D-Printed Polymer Matrix Composites Reinforced With Discontinuous Fibers,” *Solid Free. Fabr. 2019 Proc. 30th Annu. Int. Free. Fabr. Symp. – An Addit. Manuf. Conf. Process. Charact. 3D-PRINTED Polym. MATRIX Compos. Reinf. WITH DIS*, no. January, pp. 1054–1066, 2019.

[31] A. Nasirov and I. Fidan, “Graphical Abstract Prediction of Mechanical Properties of Fused Filament Fabricated Structures via Asymptotic Prediction of Mechanical Properties of Fused Filament Fabricated Structures via Asymptotic.”

[32] A. Nasirov, S. Hasanov, and I. Fidan, “Prediction of Mechanical Properties of Fused Deposition Modeling Made Parts Using Multiscale Modeling and Classical Laminate Theory,” *Proc. 30th Annu. Int. Solid Free. Fabr. Symp. Addit. Manuf. Conf. Austin, TX*, no. December, pp. 1373–1382, 2019.

[33] A. Nasirov, A. Gupta, S. Hasanov, and I. Fidan, “Three-scale asymptotic homogenization of short fiber reinforced additively manufactured polymer composites,” 2020.

[34] S. Ford and M. Despeisse, “Additive manufacturing and sustainability: an exploratory study of the advantages and challenges,” *J. Clean. Prod.*, vol. 137, pp. 1573–1587, Nov. 2016.

[35] A. B. Spierings, T. L. Starr, and K. Wegener, “Fatigue performance of additive manufactured metallic parts,” *Rapid Prototyp. J.*, vol. 19, no. 2, pp. 88–94, 2013.

[36] M. K. Thompson *et al.*, “Design for Additive Manufacturing: Trends, opportunities, considerations, and constraints,” *CIRP Ann. - Manuf. Technol.*, vol. 65, no. 2, pp. 737–760, 2016.

[37] Astm E1131 − 08, “Standard Test Method for Compositional Analysis by Thermogravimetry 1,” *ASTM Int.*, vol. 08, no. Reapproved 2014, p. 6, 2015.

[38] M. Seifi, A. Salem, J. Beuth, O. Harrysson, and J. J. Lewandowski, “Overview of Materials Qualification Needs for Metal Additive Manufacturing,” *Jom*, vol. 68, no. 3, pp. 747–764, 2016.

[39] B. Maschinen, A. Investition, G. Beschaffungen, B. Ersatzbeschaffungen, and S. Mittelherkunft, “Metal 3D printing in construction: a review of methods, research, applications, opportunities and challenges C.,” pp. 1–36.

[40] “3D PRINTING IN AEROSPACE AND ITS LONG-TERM

SUSTAINABILITY," *Sep. Sci. Technol.*, 2016.

[41] R. E. Laureijs, J. B. Roca, S. P. Narra, C. Montgomery, J. L. Beuth, and E. R. H. Fuchs, "Metal additive manufacturing: Cost competitive beyond low volumes," *J. Manuf. Sci. Eng. Trans. ASME*, vol. 139, no. 8, pp. 1–9, 2017.

[42] W. E. Frazier, "Metal Additive Manufacturing: A Review," *J. Mater. Eng. Perform.*, vol. 23, no. 6, pp. 1917–1928, Jun. 2014.

[43] Ismail Fidan, "Special Issue on 21st Century Manufacturing," *Int. J. Rapid Manuf.*, vol. 9, p. 2020, 2020.

[44] M. A. Gibson *et al.*, "3D printing metals like thermoplastics: Fused filament fabrication of metallic glasses," *Mater. Today*, vol. 21, no. 7, pp. 697–702, 2018.

[45] L. Gregurić, "How Much Does a Metal 3D Printer Cost?," 2019. [Online]. Available: https://all3dp.com/2/how-much-does-a-metal-3d-printer-cost/.

[46] M. Chapiro, "Current achievements and future outlook for composites in 3D printing," *Reinf. Plast.*, vol. 60, no. 6, pp. 372–375, 2016.

[47] A. Regalado, "10 Breakthrough Technologies 2018," *MIT TECHNOLOGY REVIEW 121, no. 2*, pp. 36–47, 2018.

[48] K.-Y. Lee *et al.*, "Accuracy of three-dimensional printing for manufacturing replica teeth," *Korean J. Orthod.*, vol. 45, no. 5, p. 217, 2015.

[49] K. Kun, "Reconstruction and development of a 3D printer using FDM technology," *Procedia Eng.*, vol. 149, no. June, pp. 203–211, 2016.

[50] S. Lu and Y. Li, "Kinematic analysis and performance evaluation of the 3-PUU parallel module of a 3D printing manipulator," *2014 13th Int. Conf. Control Autom. Robot. Vision, ICARCV 2014*, pp. 1847–1852, 2014.

[51] L. Moˇ, "Building Delta Style FDM 3D Printer." pp. 1–6, 2005.

[52] M.- Volume, "International Journal of Engineering Research & Management Technology," no. December, 2018.

[53] M. Upadhyay, T. Sivarupan, and M. El Mansori, "3D printing for rapid sand casting—A review," *J. Manuf. Process.*, vol. 29, no. 1, pp. 211–220, Oct. 2017.

[54] M. M. Risitc, "Science of Sintering and its Future," 1975.

[55] J. K. Werner, "powder metallurgy process," 1961.

[56] M. Rahimian, N. Ehsani, N. Parvin, and H. reza Baharvandi, “The effect of particle size, sintering temperature and sintering time on the properties of Al-Al2O3 composites, made by powder metallurgy,” *J. Mater. Process. Technol.*, vol. 209, no. 14, pp. 5387–5393, 2009.

[57] Y. Han, J. Li, Q. Wei, and K. Tang, “The effect of sintering temperatures on alumina foam strength,” *Ceram. Int.*, vol. 28, no. 7, pp. 755–759, Jan. 2002.

[58] J. M. Jordan, “Additive manufacturing (‘3D printing’) and the future of organizational design: some early notes from the field,” *J. Organ. Des.*, vol. 8, no. 1, 2019.

[59] M. Fernandez-Vicente, W. Calle, S. Ferrandiz, and A. Conejero, “Effect of Infill Parameters on Tensile Mechanical Behavior in Desktop 3D Printing,” *3D Print. Addit. Manuf.*, vol. 3, no. 3, pp. 183–192, Sep. 2016.

[60] B. Rankouhi, S. Javadpour, F. Delfanian, and T. Letcher, “Failure Analysis and Mechanical Characterization of 3D Printed ABS With Respect to Layer Thickness and Orientation,” *J. Fail. Anal. Prev.*, vol. 16, no. 3, pp. 467–481, 2016.

[61] H. K. Rafi, T. L. Starr, and B. E. Stucker, “A comparison of the tensile, fatigue, and fracture behavior of Ti–6Al–4V and 15-5 PH stainless steel parts made by selective laser melting,” *Int. J. Adv. Manuf. Technol.*, vol. 69, no. 5–8, pp. 1299–1309, Nov. 2013.

[62] C. Buchanan, V. P. Matilainen, A. Salminen, and L. Gardner, “Structural performance of additive manufactured metallic material and cross-sections,” *J. Constr. Steel Res.*, vol. 136, pp. 35–48, 2017.

[63] K. Guan, Z. Wang, M. Gao, X. Li, and X. Zeng, “Effects of processing parameters on tensile properties of selective laser melted 304 stainless steel,” *Mater. Des.*, vol. 50, pp. 581–586, Sep. 2013.

[64] P. Bian, E. Yin, and B. Bao, “The Relation of the Uniformity of Composition and the Mainly Mechanical Properties of AlSi10Mg by Microanalysis in SLM,” *J. Phys. Conf. Ser.*, vol. 1213, no. 5, 2019.

[65] P. Mercelis and J. Kruth, “Residual stresses in selective laser sintering and selective laser melting,” *Rapid Prototyp. J.*, vol. 12, no. 5, pp. 254–265, Oct. 2006.

[66] S. Hwang, E. I. Reyes, K. sik Moon, R. C. Rumpf, and N. S. Kim, “Thermo-mechanical Characterization of Metal/Polymer Composite Filaments and Printing Parameter Study for Fused Deposition Modeling in the 3D Printing Process,” *J. Electron. Mater.*, vol. 44, no. 3, pp. 771–777, 2015.

[67] S. H. Masood and W. Q. Song, “Thermal characteristics of a new metal/polymer material for FDM rapid prototyping process,” *Assem. Autom.*, vol. 25, no. 4, pp. 309–315, Dec. 2005.

[68] S. Riecker, J. Clouse, T. Studnitzky, O. Andersen, and B. Kieback, “Fused Deposition Modeling,” 2001.

[69] “How to Succeed with 3D Printing Metal on a Desktop 3D Printer, Matterhackers.” [Online]. Available: https://www.matterhackers.com/support/how-to-succeed-with-3d-printing-metal-on-a-desktop-3d-printer.

[70] “Our materials change the way work is done throughout a range of industries and educational institutions.” [Online]. Available: https://www.thevirtualfoundry.com.

[71] H. Gong, D. Snelling, K. Kardel, and A. Carrano, “Comparison of Stainless Steel 316L Parts Made by FDM- and SLM-Based Additive Manufacturing Processes,” *JOM*, vol. 71, no. 3, pp. 880–885, Mar. 2019.

[72] S. Terry, I. Fidan, and K. Tantawi, “Dimensional Analysis of Metal Powder Infused Filament - Low Cost Metal 3D Printing,” *Solid Free. Fabr. Symp. Proc.*, 2019.

[73] S. M. Terry, “INNOVATING THE FUSED FILAMENT FABRICATION PROCESS METAL POWDER POLYLACTIC ACID PRINTING,” 2010.

[74] B. Liu, Y. Wang, Z. Lin, and T. Zhang, “Creating metal parts by Fused Deposition Modeling and Sintering,” *Mater. Lett.*, vol. 263, p. 127252, Mar. 2020.

[75] T. Wang, X. Chen, G. Q. Lu, and G. Y. Lei, “Low-temperature sintering with nano-silver paste in die-attached interconnection,” *J. Electron. Mater.*, vol. 36, no. 10, pp. 1333–1340, 2007.

[76] “the virtual foundry.” [Online]. Available: https://www.thevirtualfoundry.com/.

[77] M. T. I. Corporation, “KSL-1100X High Temperature Muffle Furnace Operation Manual,” pp. 510–525.

[78] O. Manual, “Thermo Scientific Lindberg / Blue M LGO □ 1200 ° C Box Furnaces,” 2017.

[79] P. Ma, L. Jiang, T. Ye, W. Dong, and M. Chen, “Melt free-radical grafting of maleic anhydride onto biodegradable poly(lactic acid) by using styrene as a comonomer,” *Polymers (Basel).*, vol. 6, no. 5, pp. 1528–1543, 2014.

[80] A. S. E228-95, “Standard Test Method for Linear Thermal Expansion of Solid Materials With a Vitreous,” *Methods*, vol. 08, no. C, pp. 1–7, 1995.

[81] “Copper property.” [Online]. Available: http://www.matweb.com/search/DataSheet.aspx?MatGUID=9aebe83845c04c1db5126fada6f76f7e.

[82] E9-19, “Standard Test Methods of Compression Testing of Metallic Materials at Room Temperature,” *ASTM B. Stand.*, no. site 1, pp. 1–10, 2019.

[83] Y. Ibrahim, G. W. Melenka, and R. Kempers, “Fabrication and tensile testing of 3D printed continuous wire polymer composites,” *Rapid Prototyp. J.*, vol. 24, no. 7, pp. 1131–1141, 2018.

[84] P. A. Lykov, E. V. Safonov, and A. M. Akhmedianov, “Selective laser melting of copper,” *Mater. Sci. Forum*, vol. 843, no. February, pp. 284–288, 2016.

[85] X. Xu, W. Yi, and R. German, “Densification and strength evolution in solid-state sintering Part I Experimental investigation,” *J. Mater. Sci.*, vol. 7, pp. 567–575, 2002.

[86] A. Yegyan Kumar, Y. Bai, A. Eklund, and C. B. Williams, “The effects of Hot Isostatic Pressing on parts fabricated by binder jetting additive manufacturing,” *Addit. Manuf.*, vol. 24, pp. 115–124, Dec. 2018.

[87] “Metal 3D printing via selective laser melting and direct metal deposition: Materials, properties and applications,” *Proc. Int. Conf. Prog. Addit. Manuf.*, vol. Part F1290, pp. 270–275, 2016.

[88] Y. Chen, C. O. Rios, A. Imeri, N. A. Russell, and I. Fidan, “Investigation of the tensile properties in fibre-reinforced additive manufacturing and fused filament fabrication,” *Int. J. Rapid Manuf.*, vol. 9, no. 2/3, p. 251, 2020.

[89] A. Gupta, I. Fidan, S. Hasanov, and A. Nasirov, “Processing, mechanical characterization, and micrography of 3D-printed short carbon fiber reinforced polycarbonate polymer matrix composite material,” *Int. J. Adv. Manuf. Technol.*, pp. 1–21, Apr. 2020.

VITA

Hao Lu was born on June 5th, 1992, in Heilongjiang, China. He completed the requirements and graduated with a Bachelor of Science degree in Mechanical Engineering from Tennessee Technological University in Cookeville, Tennessee on May 5th, 2017. Hao Lu received a Master of Science degree in Mechanical Engineering from Tennessee Technological University in August 2020.